Feature-Oriented Image Enhancement with Shock Filters, I

Leonid I. Rudin
and
Stanley Osher

Department of Computer Science
California Institute of Technology

Caltech-CS-TR-89-3

FEATURE-ORIENTED IMAGE ENHANCEMENT WITH SHOCK FILTERS, I

by

Leonid I. Rudin

Los Angeles, IBM Scientific Center
11601 Wilshire Blvd.
Los Angeles, CA 90025-1738

and

California Institute of Technology
Pasadena, CA 91125

Stanley Osher

Cognitech Inc.
426 Lincoln Boulevard
Santa Monica, CA 90402

and

Department of Mathematics
University of California
Los Angeles, CA 90024-1555

Caltech-CS-TR-89-3

I. Introduction.

A basic step in the processing of signals (images, radar, acoustic signals) is enhancement. By this we mean the removal of blurring.

An elementary example of blurring comes from the degradation of a signal through some kind of convolution. More precisely, let

$$x = (x_1, \ldots, x_n)\ \varepsilon R^n$$

and let $u_0(x)$ be the original real valued function which is blurred through convo-

lution with a kernel: $j(x)$

$$w(x) = j \star u_0 = u_0 \star j = \int_{R^n} j(x-y)u_0(y)dy. \tag{1.1}$$

Typically, j has the following properties

$$j(x) \geq 0$$

$$j(x) \to 0 \text{ rapidly as } |x| \to \infty, \text{ where } |x| = (x_1^2 + x_2^2, \ldots, x_n^2)^{\frac{1}{2}} \tag{1.2}$$

$$\int_{R^n} j(x)dx = 1.$$

Examples include for any $t > 0$:

(1.3a) $j^{(1)}(x) = \frac{1}{(4\pi t)^{\frac{n}{2}}} e^{-\frac{|x|^2}{4t}}$ (the heat kernel)

(b) $j^{(2)}(x) = j^{(2)}(|x|)$,

$j^{(2)}(|x|)$ is strictly decreasing with $|x|$, for $|x| < 1$

$j^{(2)}(|x|) \equiv 0$ if $|x| \geq 1$

$j \in C^\infty$

Then consider for any $\delta > 0$

$$j_\delta^{(2)} = \frac{1}{\delta^n} j^{(2)}(\frac{|x|}{\delta})$$

we call $j_\delta^{(2)}$ a "mollifying" kernel.

(c) $j_\delta^{(3)}(x) \equiv \frac{1}{\delta^n} \quad \{x / -\frac{\delta}{2} \leq x_i \leq \frac{\delta}{2}, \quad i = 1, \ldots, n\}$

$j_\delta^{(3)}(x) \equiv 0$ otherwise

$j_\delta^{(3)}$ is the "box" kernel.

If we take the Fourier transform of (1.1) we arrive at

$$\hat{w}(\xi) = \hat{j}(\xi)\hat{u}_0(\xi) \tag{1.4}$$

To recover $u_0(x)$, we need to deconvolve, i.e. to reverse the procedure in (1.1). From (1.4), this amounts to dividing by $\hat{j}(\xi)$ and applying the inverse Fourier transform. The problem with this procedure, of course, is that this is generally very ill-posed. Since j is usually relatively smooth, $\hat{j}(\xi) \to 0$ rapidly as $|\xi| \to \infty$, and large frequencies in $\hat{w}(\xi)$ get amplified considerably.

The function $u_0(x)$ is often taken to be band limited, i.e. $\hat{u}_0(\xi) \equiv 0$ for $|\xi|$ large enough, say for $|\xi_i| > N$ for each $i = 1, \ldots, n$. An important example of this comes through discretization. Let $u_h(x)$ be a grid function defined at grid points

$$\begin{aligned} &(x_i)_\ell = \ell h, \\ &i = 1, \ldots, n; \quad \ell = (\ell_1, \ldots, \ell_n) \\ &\ell_i = 0, \pm 1, \ldots, \pm N; \quad (2N+1)h = 1 \end{aligned} \tag{1.5}$$

and suppose u_h is extended to be periodic on the grid with

$$u_h(x + e_i) \equiv u_h(x)$$

for each $e_i = (0, 0, \ldots, 1, 0, \ldots, 0)$, where the 1 occurs in the i^{th} component, $i = 1, \ldots, N$.

The grid function has a unique trigeometric interpolant

$$Iu_h(x) = \Sigma(\tilde{u}_h)_\ell e^{i\ell \cdot x} \tag{1.6}$$

where the sum is taken over the cube: $-N \leq \ell_i \leq N$, $i = 1, \ldots, N$ and

$$Iu_h(x_\ell) = u_h(x_\ell) \tag{1.7}$$

for each grid point x_ℓ.

See, e.g., [7] for a description of this interpolant and its properties.

Thus deconvolution on a grid amounts to multiplying each discrete Fourier coefficient $(\tilde{u}_h)_\ell$ by $(\hat{j}(\ell))^{-1}$. This number typically grows like $|\ell|$ to some positive power, or even like the exponential of a positive power of $|\ell|$. If u_h is the discretization of a very smooth function, then the coefficients $(\tilde{u}_h)_\ell$ decay rapidly – perhaps more rapidly than the growth in $(\hat{j}(\ell))^{-1}$. However, there is generally high frequency noise in all this, i.e., the discretization itself can well introduce non-smooth, but low amplitude, round-off errors. Deconvolution in this simple fashion will amplify this noise in a very unstable manner.

The situation is far worse if the underlying function u_0, which is sampled on grid points, is only piecewise continuous – if it has jumps or jumps in derivatives. Then there exist two problems.

The first is global. It was shown in [9] that there is a *global* error between the interpolant Iu_h and u_0 which is e.g., $O(h)$ for functions which have jumps. This is true globally, i.e. at any finite distance from the discontinuity. More seriously, any attempt to approximate u_0 by either a Fourier interpolant Iu_h, or a truncated Fourier transform of u_0 – e.g. by considering

$$\hat{\rho}(\xi)\ \hat{u}_0(\xi) \tag{1.8}$$

for

$$\hat{\rho}(\xi) \equiv 1 \text{ if } |\xi| \leq m_1$$

$$\hat{\rho}(\xi) \equiv 0 \text{ if } |\xi| > m_2$$

will lead to Gibbs' phenomena. These are 0(1) errors near the discontinuity in $u_0(x)$, which do not disappear as $m_1,\ m_2 \to \infty$ (or $h \downarrow 0$). These errors cause the well

known phenomenon of "ringing" in image processing. This is particularly problematic for the machine processing of images. Thus, an attempt to deconvolve without amplifying high frequency errors due to noise, by cutting off the high frequencies, will lead to severe oscillations near the discontinuities of the original function u_0.

The procedures discussed so far are all linear and/or all involve the Fourier transform of u_0. This way of thinking is inherently problematic for the processing of images which are only piecewise smooth.

We remark that feature dependent image processing was tried in [18]. There they used a filter which is the sum of two components – a linear low pass and a linear high pass filter. This leads to a generally oscillatory procedure of limited practical value. It does, however, represent a first attempt to perform a context sensitive enhancement.

It was pointed out in [14], [15] that images are dominated by the geometry of their features – edges, corners, etc. In fact the space of functions of bounded variation appears to be the correct class for image analysis.

In [14] the concepts and techniques developed in the numerical solution of nonlinear hyperbolic equations were applied for the first time to feature oriented image enhancement. There the first experimental shock filter, based on a modification of the nonlinear Burgers' equation was used. (See the Appendix). However this first shock filter did not incorporate the crucial feature-detector switch, the TVD computational approach, and the theoretical basis developed herein.

Both subjects (image enhancement; shock calculations) deal with the discrete representation of discontinuous functions. The relevant concepts include: characteristic speed, variation diminishing or essentially non-oscillatory approximations,

the need for nonlinear approximations to linear problems, compressive methods. See, e.g. [1], [13] for overviews of this subject.

In this paper, the first of a series, we shall develop shock filters for image enhancement. The filters use nonlinear time dependent partial differential equations. The evolution of the initial data $u_0(x)$ into a steady state solution $u_\infty(x)$ as $t \to \infty$ through $u(x,t)$, $t > 0$, is the filtering process. The partial differential equations have solutions which satisfy a maximum principle and more. In fact the total variation of the solution for any fixed positive time is the same as that of the initial data, i.e. the operator is total variation preserving. The steady state solution is achieved relatively quickly in most cases, and this is the processed image. The initial data is, of course, the discretization of the original image.

The processed image is piecewise smooth. In fact it is a solution of any one of a class of second order elliptic partial differential equations in regions of smoothness. The jumps occur across the zeros of the elliptic operator applied to the initial data. The essential features of the true image are recovered in many cases – these include: number of jumps, relative size of jumps, and location of jumps. In some, more special cases, given the knowledge of the method of blurring, our results can be made exact, if the blurring (e.g. δ in equation (1.2b)) is not too large.

We shall draw from experience in the numerical solution of hyperbolic problems which have discontinuous solutions. Such a problem is exemplified by a scalar conservation law

$$u_t + f(u)_x = 0 \tag{1.9a}$$

to be solved for $-\infty < x < \infty (x \epsilon R^1)$, $t > 0$ with initial data:

$$u(x,0) = u_0(x) \tag{1.9b}$$

If $f'' \not\equiv 0$, then the solution generally develops discontinuities even for very smooth $u_0(x)$.

For a small time the solution is constant along characteristics; i.e.

$$u(x,t) = u_0(x - f'(u)t) \tag{1.10}$$

for t sufficiently small. This means that u is constant along characteristics: $x - f'(u)t =$ constant. In finite time these characteristics generally intersect and shocks develop, i.e. the solution becomes a weak solution. This solution is typically piecewise continuous with jumps across curves satisfying

$$\frac{dx}{dt} = \frac{[f]}{[u]}$$

whose [ ] denotes the jump across the curve.

The modern way to solve this problem numerically uses a shock-capturing method. The solution, shocks and all, is obtained through a single, globally defined algorithm.

One approximates (1.8) by setting up a grid: $x_i = ih, \quad t^n = n\Delta t$

$$i = 0, \pm 1, \pm 2 \ldots, \quad n = 0, 1, \ldots$$

A shock capturing approximation is, by definition, in conservation form:

$$u_i^{n+1} = u_i^n - \frac{\Delta t}{n}(g^n_{i+\frac{1}{2}} - g^n_{i-\frac{1}{2}}) \tag{1.11}$$

where (1.12) $g^n_{i+\frac{1}{2}} = g(u^n_{i-k}, \ldots, u^n_{i+k+1})$ is the numerical flux approximating $f(u)$; g is Lipschitz continuous with:

$$g(u, u, \ldots, u) = f(u)$$

This guarantees that bounded almost everywhere convergent sequences of solutions to (1.11) will yield weak solutions of (1.9) [8].

Of course much more than conservation form is needed for a good scheme. Obvious issues involve stability and convergence. A more subtle issue involves accuracy in the presence of discontinuities. Schemes which are simple (e.g. linear if $f(u)$ is linear, $f(u) = au$) and which do not generate oscillations near discontinuities of the solution, must of necessity, be only first order accurate (see e.g. [2], [6]). Thus they smear discontinuities badly.

A great deal of successful work has been done to overcome this limitation. See, e.g. [5], [16], [17]. The goal is to get highly accurate (in regions of smoothness) methods which resolve discontinuities sharply and accurately in a non-oscillatory way. In the next sections we shall borrow ideas from shock calculations, modify them appropriately, and apply them to image enhancement.

The format of this work is as follows.

In section II, we shall discuss a one dimensional enhancement procedure. We set up a new partial differential equation (PDE) which acts as our enhancement filter and describe its (surprising) properties. We then set up a total variation preserving (TVP) approximation to this PDE, describe its properties, and perform numerical experiments.

In section III, we extend the procedure of section II to two space dimensions, i.e. to real images. The rigorous mathematical theory of this problem in two dimensions, is not as extensive. Nevertheless the numerical schemes yield the described enhancement features. This will be demonstrated again by numerical experiments on real pictures in section IV.

A big difference between one and two dimensions comes in the freedom of choice one has, in which second order elliptic operator to use in the enhancement PDE. This is equivalent to the choice of edge detector one uses. The zeros of this operator (generalized inflection points) applied to the initial data will give us the location of the edges of our enhanced image. The final enhanced image will be a piecewise smooth function which satisfies the homogeneous elliptic equation in regions of smoothness.

Finally, in an appendix we discuss the relation between the present method and that earlier developed in [15].

II. One Dimensional Enhancement.

We begin by considering the equation

(2.1a) $$u_t = -|u_x|\ F(u_{xx})$$

to be solved for all x, $t \geq 0$ with initial data:

(2.1b) $$u(x,0) = u_0(x)$$

Here the Lipschitz continuous function F satisfies

(2.1c)

(i) $F(0) = 0$

(ii) $X(u)F(u) > 0, \quad u \neq 0$

where $X(u) = 1$ if $u > 0$, $X(u) = -1$ if $u < 0$, $X(0) = 0$.

An example is:

(2.2) $$u_t = -|u_x|\, u_{xx}$$

This looks at first like an extremely ill-posed problem. The coefficient of u_{xx} is never positive. In fact it is negative except at extrema of u where it vanishes. This initial value problem turns out to be well-posed, or at least to satisfy the following á priori estimates (which are true for (2.1) with general F satisfying (2.2))

(2.3)

(i) $TV\ u(\cdot,t) = TV\ u_0(\cdot)$

(ii) $\max u(\cdot,t) = \max u_0(\cdot)$

(iii) $\min u(\cdot,t) = \min u_0(\cdot)$

We can best exemplify the behavior of this enhancement procedure by taking a case which is outside our definition, in that F is not Lipschitz continuous. Let $F(u) = X(u)$.

Then u satisfies:

(2.4a) $$u_t = \pm u_x \text{ if } u_{xx} \neq 0$$

(b) $$u_t = 0 \text{ if } u_{xx} = 0$$

We thus have a simple linear advection equation in which the direction of propagation changes sign or becomes zero at extreme and inflection points of u. An interesting example comes from taking

(2.4c) $$u_0(x) = \cos x$$

Then

(2.5a)
$$u(x,t) = \cos(x-t) \text{ for } t < x < \frac{\pi}{2}$$
$$u(x,t) = 1 \text{ for } -t < x < t$$
$$u(x,t) = \cos(x+t) \text{ for } -\frac{\pi}{2} < x < -t$$

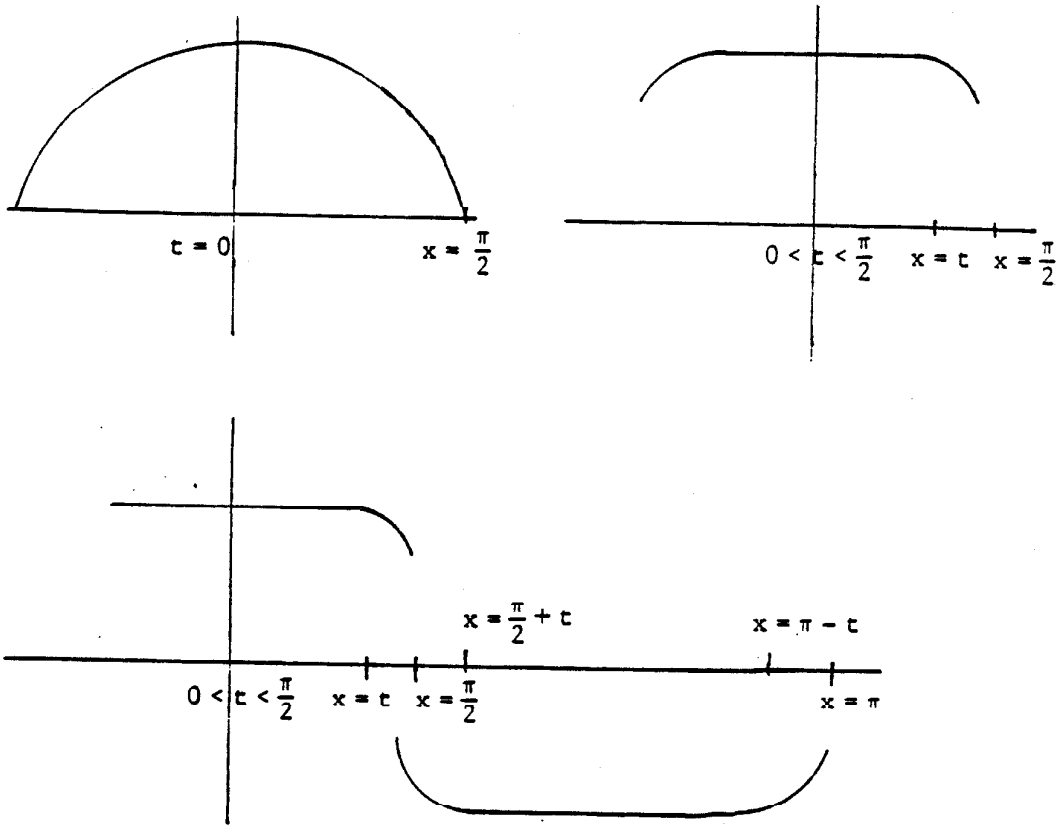

Figure 2.1

By symmetry, discontinuities develop at $x = (2k+1)\frac{\pi}{2}$, $k = 0, \pm 1, \pm 2, \ldots$.

Finally at $t = \frac{\pi}{2}$ and for all $t > \frac{\pi}{2}$, the enhanced image is:

$$u_\infty = (-1)^k \text{ for } (2k-1)\frac{\pi}{2} < x < (2k+1)\frac{\pi}{2}.$$

To show that the transformation

$$u_0 \rightarrow u_\infty$$

is an approximate deconvolution, we consider what it does to convolution of a step function by $j_\delta^{(2)}(x)$ as defined in (1.3b).

Let $w(x)$ be a step function with values

$$w(x) \equiv w_\nu \text{ in } I_\nu = \{x / x_{\nu-\frac{1}{2}} \leq x < x_{\nu+\frac{1}{2}}\} \tag{2.6}$$

where the real line is the union of all these I_ν's. Let $0 < d = \inf_\nu [x_{\nu+\frac{1}{2}} - x_{\nu-\frac{1}{2}}]$. Finally, take $0 < \delta < \frac{d}{2}$ be given.

Define

$$u_0 = j_\delta^{(2)} * w. \tag{2.7}$$

It is easy to see that

$$u_0(x) \equiv w_\nu \text{ for } x_{\nu-\frac{1}{2}} + \delta < x < x_{\nu+\frac{1}{2}} - \delta.$$

$$u_0'(x) = (w_{\nu+1} - w_\nu) j_\delta^{(2)}(x - x_{\nu+\frac{1}{2}})$$

$$\text{for } x_{\nu+\frac{1}{2}} - \delta < x < x_{\nu+\frac{1}{2}} + \delta$$

$$u_0''(x) = (w_{\nu+1} - w_\nu) j_\delta^{(2)'}(x - x_{\nu+\frac{1}{2}})$$

Thus, for x between $x_{\nu+i} - \delta$ and $x_{\nu+\frac{1}{2}} + \delta$, u_0 moves strictly monotonically from w_ν to $w_{\nu+1}$ after which it becomes constant until x reaches $x_{\nu+\frac{3}{2}} - \delta$. Also u_0 has only one inflection point in this interval, and that is at $x = x_{\nu+\frac{1}{2}}$. We have

THEOREM 2.1. *If $F = X$ in* (2.1a), *then the transformation $u_0 \to u_\infty$ with $u_0 = j_\delta^{(2)} * w$ for $\delta < \frac{d}{2}$ yields $u_\infty = w$ where w is the step function defined in* (2.6). *Thus the shock filter is an exact deconvolution in this case.*

REMARK (2.1). We are tacitly assuming that the discontinuities developing in equation (2.1) occur exactly where we want them – at inflection points of the initial

data, where the characteristics intersect. This is borne out by all our numerical experiments.

REMARK (2.2). In [15] the analog to (2.1a) was

$$u_t = +|u_x|u. \tag{2.8}$$

Now if u is initially a trigonometric function, e.g., $u = \sin x$, then $u_{xx} = -u$ and initially we arrive at (2.2). This is discussed further in the appendix below.

Our theory for solutions to (2.1) comes from the following. If we differentiate (2.1) with respect to x, multiply by $X(u_x)$ and integrate the result with respect to x, we arrive at

$$\begin{aligned} \frac{\partial}{\partial t}\int |u_x| &= -\int \frac{\partial}{\partial x}(u_x\ F(u_{xx})) \\ &= 0 \end{aligned} \tag{2.9}$$

if u is eventually constant for $|x|$ large. This proof is rigorously true as long as u stays smooth. Moreover, our discrete approximation has this property for general initial data. Thus we conjecture:

CONJECTURE 2.1. The evolution equation, (2.1), with $u_0(x)$ continuous, has a unique solution $u(x,t)$ which has jumps only at inflection points of $u_0(x)$. The total variation in x of $u(x,t)$ is invariant in time, as are the location and value of local extrema.

We now set up a discrete approximation to (2.1) which preserves the variation and the size and location of extrema. We approximate (2.1) by

$$u_i^{n+1} = u_i^n - \frac{\Delta t}{h}|m(\Delta_+ u_i^n, \Delta_- u_i^n)|F(\frac{\Delta_+\Delta_- u_i^n}{h^2}) \tag{2.10a}$$

Here $m(x,y)$ is the minmod function defined by

$$m(x,y) = \begin{cases} (\text{sign } x)\min(|x|,|y|) & \text{if } xy > 0 \\ 0 & \text{if } xy \le 0 \end{cases} \tag{2.10b}$$

and

$$\Delta_{\pm} u_i = \pm(u_{i\pm1} - u_i) \tag{2.10c}$$

Call $F\left(\frac{\Delta_+\Delta_- u_i^n}{h^2}\right) = F_i^n$. Then

$$\begin{aligned} \Delta_+ u_i^{n+1} = \Delta_+ u_i^n &- \frac{\Delta t}{h}|m(\Delta_+ u_{i+1}^n, \Delta_+ u_i^n)|\ F_{i+1}^n \\ &+ \frac{\Delta t}{h}|m(\Delta_+ u_i^n, \Delta_- u_i^n)|\ F_i^n \end{aligned} \tag{2.11}$$

We require (CFL restriction)

$$\sup_i \frac{\Delta t}{h} F_i^0 \le \frac{1}{2}.$$

It is now easy to see that the right side of (2.6) has the same sign as $\Delta_+ u_i^n$ (and vanishes if $\Delta_+ u_i^n = 0$). Thus we have

$$\begin{aligned} |\Delta_+ u_i^{n+1}| = |\Delta_+ u_i^n| &- \frac{\Delta t}{h}\chi_{i+\frac{1}{2}}^n |m(\Delta_+ u_{i+1}^n, \Delta_+ u_i^n)| F_{i+1}^n \\ &+ \frac{\Delta t}{h}\chi_{i+\frac{1}{2}}^n |m(\Delta_+ u_i^n, \Delta_- u_0^n)| F_i^n, \end{aligned} \tag{2.12}$$

where

$$\chi_{i+\frac{1}{2}}^n = \text{sign } \Delta_+ u_i^n.$$

By the definition of the minmod function, it follows that

$$\chi_{i+\frac{1}{2}}^n |m(\Delta_+ u_{i+1}^n, \Delta_+ u_i^n)| = \chi_{i+\frac{3}{2}}^n |m(\Delta_+ u_{i+1}^n, \Delta_+ u_i^n)| \tag{2.13}$$

Thus we arrive at:

$$|\Delta_+ u_i^{n+1}| = |\Delta_+ u_i^n| - \frac{\Delta t}{h}\Delta_+(\chi_{i+\frac{1}{2}}^n) m|(\Delta_+ u_i^n, \Delta_- u_i^n)| F_i^n$$

Finally

$$TV(u^{n+1}) = \sum |\Delta_+ u_i^{n+1}| = \sum |\Delta_+ u_i^n| = TV(u^n) \tag{2.15}$$

This is a total variation preserving (TVP) method. Moreover, if $u_{i_0}^{n+1}$ is a local maxima for u_i^{n+1}, then since sign $\Delta_+ u_{i_0}^{n+1}$ = sign $\Delta_+ u_{i_0}^n$ and sign $\Delta_- u_{i_0}^{n+1}$ = sign $\Delta_- u_{i_0}^n$, then $u_{i_0}^n$ is a local maxima for u_i^n. By the definition of minmod it follows that

$$u_{i_0}^{n+1} = u_{i_0}^n.$$

The same is true for $u_{i_0}^{n+1}$, a local minima. We now have

THEOREM 2.2. *The scheme* (2.10) *enforces a local maximum and minimum principle - in fact such local extrema remain unchanged in time. Moreover the scheme is TVP.*

Thus, for fixed $\Delta t, h$, as $n \to \infty$ the sequence of discrete solutions has a convergent subsequence. We believe this limit to be unique and we call the conjectured unique limit $(u^\infty)_h$ the discrete processed image.

As $\Delta t \to 0$, $h \to 0$, the sequence of discrete solutions also has a convergent subsequence. We again believe this limit to be unique – this is the continuum processed image.

Let

$$\max(x, 0) = x^+$$

$$\min(x, 0) = x^-$$

Then it turns out that we may rewrite (2.10a) equivalently as

$$\begin{aligned} u_i^{n+1} = u_i^n &- \frac{\Delta t}{h}\sqrt{((\Delta_+ u_i)^+)^2 + ((\Delta_- u_i)^-)^2}(F_i^n)^- \\ &- \frac{\Delta t}{h}\sqrt{((\Delta_+ u_i)^-)^2 + ((\Delta_- u_i)^+)^2}(F_i^n)^+ \end{aligned} \tag{2.16}$$

If we (mentally) fix the value of F_i^n to be constant c, then (2.16) is Godunov's method approximating

$$u_t = -|u_x|c \tag{2.17}$$

see e.g. [2], [11]. We chose this method because, among three point approximations to (2.17) which are monotone, this is the most compressive, i.e. least dissipative [11]. This scheme (2.16) is almost monotone in the sense that if $(F_i^n)^-$ is a fixed constant ≤ 0 or $(F_i^n)^+$ is a fixed constant ≥ 0, then the right hand side is a non-decreasing function of the u_i^n.

In a sense our difference operator is too compressive. Isolated extrema are unchanged. The procedure, for example does not remove "salt and pepper effects". In succeeding papers, we shall correct this.

It is easy to see that discrete piecewise constants are left invariant by (2.10). So are piecewise linear, continuous profiles with extrema coinciding with the "kinks", i.e. jumps in derivative. In order to accept general piecewise linear functions we may modify F_i^n.

Let

$$\tilde{F}_i^n = F(m[\frac{\Delta_-\Delta_- u_i^n}{h^2}, \frac{\Delta_-\Delta_+ u_i^n}{h^2}, \frac{\Delta_+\Delta_+ u_i^n}{h^2}]) \tag{2.18}$$

where minmod of n numbers is defined by inductions

$$m[(x^1, x^2, \ldots, x^n)] = m[(x^1, \ldots, x^{n-1}), x^n] \tag{2.19}$$

Our modified scheme is:

$$u_i^{n+1} = u_i^n - \frac{\Delta t}{h}|m[\Delta_- u_i^n, \Delta_+ u_i^n]|\tilde{F}_i^n \tag{2.20}$$

Results of One-Dimensional Implementation of the Shock Filter.

We now present the computed time evolution of one-dimensional wave forms acted upon by the shock filter described by the scheme (2.10a).

Plots 1(a) - 1(e) demonstrate the enhancement procedure applied to the function of 1(b) which is a slightly diffused version of the sinusoid in Plot 1(a). The evolution procedure with stationary inflection points which correspond here to zeros of the function, eventually produces a steady state 1(e) which is a "square wave". Observe that the transformation is a continuous process, for otherwise, by knowing the TVP nature of the equation (2.1a) one could have done the same just by finding inflection points, and extrema and then performing thresholding. However such an algorithm would result in futile exercise if one tried to extend it to a 2-dimensional calculation. Furthermore equation (2.1a) will be generalized in subsequent paper to include reconstruction of higher derivatives i.e. allow growth of the extrema (losing the TVP property) hence no thresholding could give the desired enhancement (which could be enhancements of higher derivatives).

The sequence Plot 2(a) - 2(f) demonstrates that the edge development process is not necessarily producing smooth wave-forms culminating in a piecewise constant function, but also that breaks in derivatives ("kinks") do develop (see 2(b)). The edge-switch F in (2.10(a)) of this example had been taken to be

$$F = \text{sign}\,(\Delta_+\Delta_- u_i^n) \tag{2.21}$$

One has to be warned that various other choices of F may result in an unpleasant numerical "freeze up" behavior such as on Plot 3 where the edge-switch was taken to be normalized second derivative. There Plot 3 is actually of a steady-state result.

On the other hand replacing $m(x, y)$ in (2.10a) with any more compressive function renders the scheme unstable and blows up quite rapidly – Plot 4.

Again the significance of the 1-dimensional filter is not just necessarily the steady state result, but the continuous process it produces. Incidentally we intend to experiment with this class of filters on one-dimensional speech-wave forms to determine if any perceptible speech enhancement results. In this case the transitory solution is of interest.

Two Dimensional Enhancement.

We now consider the equation

$$u_t = -\sqrt{u_x^2 + u_y^2}F(\mathcal{L}(u)) \tag{3.1a}$$

to be solved for all x, y, and for $t \geq 0$, with initial data

$$u(x, y, 0) = u_0(x, y) \tag{3.1b}$$

Here $F(u)$ satisfies (2.1c). Also $\mathcal{L}(u)$ is a second order, (generally) nonlinear elliptic operator.

The general idea for the construction of the multi-dimensional shock filter should be evident by now.

In both of the equations (2.1a) and (3.1a) we have nonlinear combination of the propagation term: $|\nabla u|$-magnitude of the gradient, and an edge-detection term $F(\mathcal{L}(u))$ whose desired behavior involves changing sign across any essential singular feature. Thus edge formation and sharpening process will occur at the places where

$$\mathcal{L}(u) = 0 \tag{3.2a}$$

Thus the choice of $\mathcal{L}(u)$ is governed by how faithfully the zero-crossings of this differential operator define edges of the processed image.

The (well know in computer vision literature) scheme due to D. Marr, works by finding zeros of

$$\mathcal{L}(u) = \nabla^2(u(x,y) * G(x,y)) \tag{3.2b}$$

where $G(x,y)$ is a two-dimensional Gaussian. Since the function we are processing has already been blurred, i.e. convolved with a Gaussian, the choice for edge operator would be

$$\mathcal{L}(u) = u_{xx} + u_{yy} \qquad \text{(the Laplacian)} \tag{3.2c}$$

The reader is referred to [15] for the rigorous local analysis of this and a host of other edge-detectors. In [15] an analytical tool (called the numerical analysis of singularities) is developed in order to evaluate the behavior of "feature detectors" in the vicinity of singularities. There it is shown that the detector (3.2c) will entirely miss any nontrivial singular boundaries and, since the generalized Laplacian does not contain any curvature-dependent term, it is curvature insensitive. A somewhat better version of (3.2c) is a scheme in which edges are extracted from the zero crossings of second directional derivatives [4]. We shall skip the polynomial approximation of [4] and simply set

$$\mathcal{L}(u) = u_{xx} \cdot u_x^2 + 2 \cdot u_{xy} u_x u_y + u_{yy} \cdot u_y^2 \tag{3.2d}$$

which is simply an expression for the second derivative of u in the direction of the gradient.

We numerically implement (3.2d) by

$$F(u) = (\Delta_+^x \Delta_-^x u)[m(\Delta_+^x u, \Delta_-^x u)]^2 + \Delta_+ \Delta_- u \cdot [m(\Delta_+^y u, \Delta_-^y u)]^2$$
$$+ (\Delta_-^x \Delta_-^y u + \Delta_+^x \Delta_+^y u)(m(\Delta_+^x, \Delta_-^x u))m(\Delta_+^y u, \Delta_-^y u) \tag{3.2e}$$

We finally normalize $F(u)$ by

$$\tilde{F}(u) = \frac{F(u)}{1 + |F(u)|} \tag{3.2f}$$

It should be noted here that the enhancement procedure is only as good as the quality of the feature detector it utilizes. The choice of (3.2d) is governed by a compromise between quality of filtering and the computational complexity limitations, for the shock filter needs to recompute the "edge-switch" in the beginning of each iteration.

Greatly superior quality of enhancement should result from the kind of local feature detectors proposed in [15]. A demonstration of the highest precision of this scheme is given in the computer-generated "pencil drawing" of the "Tank" picture 0. However this will require a much more powerful interactive graphics facility than is available to the authors at the moment.

The estimate analogous to that in (2.9) is unfortunately lacking here. We rederive a result used in [3] here.

Let ∇ and $\nabla\cdot$ denote gradient and divergence respectively. Let $|(x_1, x_2)| = \sqrt{x_1^2 + x_2^2}$.

We wish to compute

$$\frac{\partial}{\partial t}|\nabla u| = \frac{\nabla u}{|\nabla u|}\cdot(u_{xt}, u_{yt}) \tag{3.3}$$

$$= \left(\frac{u_x}{|\nabla u|}\frac{\partial}{\partial x} + \frac{u_y}{|\nabla u|}\frac{\partial}{\partial y}\right)(-|\nabla u| F(\mathcal{L}(u))$$

$$= -\nabla\cdot(F(\mathcal{L}(u))\nabla u)$$

$$+ F(\mathcal{L}(u))|\nabla u|\left(\nabla\cdot\left(\frac{\nabla u}{|\nabla u|}\right)\right)$$

$$= -\nabla\cdot(F(\mathcal{L}(u))\nabla u)$$

$$- |\nabla u|\mathcal{K}(u)F(\mathcal{L}(u))$$

Here $\mathcal{K}(u)$ is the curvature of level sets, u = constant

$$\mathcal{K}(u) = -\nabla\cdot\left(\frac{\nabla u}{|\nabla u|}\right) \tag{3.4}$$

$$= -\left(\frac{u_{xx}u_y^2 - 2u_{xy}u_x u_y + u_{yy}u_x^2}{|\nabla u|^3}\right)$$

If we integrate both sides of (3.3) over R^2, we arrive at:

$$\frac{\partial}{\partial t}\int_{R^2}|\nabla u| = \frac{\partial}{\partial t}TV|u| \tag{3.5}$$

$$= -\int_{R^2}|\nabla u|\mathcal{K}(u)F(\mathcal{L}(u))$$

For this evolution procedure to be TV bounded at any positive time, it suffices that $-\mathcal{K}(u)F(\mathcal{L}(u))$ be bounded above. Unfortunately, such an estimate is not generally true.

Parenthetically, we note that if $\mathcal{L}(u) = \mathcal{K}(u)$ (which makes (3.1) anticompressive), then we are computing level surfaces of a curve being deformed under its mean curvature, see [3], [12]. We have rederived here in (3.5) a dissipative estimate – decay of variation in this case.

We shall approximate (3.1) by setting up a grid

$$x_i = ih_1,\ y_j = jh_2,\ t^n = n\Delta t.$$

$$i, j = 0, \pm 1, \pm 2, \ldots, n = 0, 1, 2, \ldots$$

For simplicity of exposition, we shall take $h_1 = h_2 = h$. The approximate solution is to satisfy:

$$u_{ij}^n \approx u(ih, jh, n\Delta t)$$

Our first approximation is

$$(3.6a)\quad u_{ij}^{n+1} = u_{ij}^n - \frac{\Delta t}{h}\sqrt{(m(\Delta_+^x u_{ij}^n, \Delta_-^x u_{ij}^n))^2 + (m(\Delta_+^y u_{ij}^n, \Delta_-^y u_{ij}^n))^2}F_{ij}(\mathcal{L}(u^n))$$

Here we have defined $\Delta_\pm^x, \Delta_\pm^y$ to be the forward and backwards difference operators in the x and y directions. Also $F_{ij}(\mathcal{L}(u)) = F(\mathcal{L}_{ij}(u))$ where $\mathcal{L}_{ij}$ is a discretization of the second order edge detector, using central differencing for u_{xx} and u_{yy}, i.e. $u_{xx} \approx \frac{1}{h^2}\Delta_+^x\Delta_-^x u_{ij}$, etc., symmetric differencing for $u_{xy} \approx \frac{1}{2h^2}(\Delta_-^x\Delta_-^y + \Delta_+^x\Delta_+^y u)$ and the u_x, u_y terms (if needed) are approximated using the minmod operator.

The CFL restriction is

$$(3.6b)\qquad \sup\frac{\Delta t}{h}F_{ij}(\mathcal{L}(u^0)) \le \frac{1}{4}$$

A slight modification of this scheme comes from

$$(3.7)$$
$$u_{ij}^{n+1} = u_{ij}^n - \frac{\Delta t}{h}\sqrt{((\Delta_+^x u_{ij}^n)^+)^2 + ((\Delta_-^x u_{ij}^n)^-)^2 + ((\Delta_+^y u_{ij}^n)^+)^2 + ((\Delta_-^y u_{ij}^n)^-)^2}F_{ij}^-(\mathcal{L}(u^n))$$
$$- \frac{\Delta t}{h}\sqrt{((\Delta_+^x u_{ij}^n)^-)^2 + ((\Delta_-^x u_{ij}^n)^+)^2 + ((\Delta_+^y u_{ij}^n)^-)^2 - ((\Delta_-^y u_{ij}^n)^+)^2}F_{ij}^+(\mathcal{L}(u^n))$$

with the same CFL restriction (3.5b).

Our only rigorous theoretical results here are the following:

(A) For (3.6a): If $u^n_{i_0 j_0}$ is a local maximum

$$u^n_{i_0 j_0} \geq \max(u^n_{i_0-1,j_0}, u^n_{i_0+1,j_0}, u^n_{i_0,j_0-1}, u^n_{i_0,j_0+1})$$

then it is not enhanced – in fact

$$u^{n+1}_{i_0 j_0} = u^n_{i_0 j_0}$$

The same is true for local minima.

(B) For (3.7): For fixed constant values of $F^-_{ij} \leq 0$ and $F^+_{ij} \geq 0$, then the scheme is monotone – the right hand side of (3.7) is a nonincreasing function of its arguments.

We also consider an option which replaces $F_{ij}(\mathcal{L}(u^n))$ by $\tilde{F}_{ij}(\mathcal{L}(u^n))$

$$\tilde{F}_{ij} = F(m[\mathcal{L}_{i+\nu,j+\mu}(u^n)])$$
$$\nu, \mu = -1, 0, 1.$$

Thus the processing will leave invariant piecewise continuous approximate solutions of

$$\mathcal{L}(u) = 0$$

4. Results of Two-Dimensional Implementation of the Shock Filter.

We demonstrate the shock filtering enhancement scheme (3.7) on various standard images from the USC IPI Image Data Base. In this experiment we first blur a picture with number N_d of iterations of a standard approximation of the diffusion equation (4.1)

(4.1) $$u_t = K \cdot \Delta u$$

where K is chosen to be the largest satisfying the stability criteria, i.e. $K = .25$. Then we show a few iterations of the shock filter N_s with the final one at steady state. The CFL # = .25, the maximal possible under the stability restriction. There are 256 gray levels for each picture element (pixel). Hence the quantization error is $\sim 4 \times 10^{-3}$. If simple reversal of the equation (4.1) is attempted, the image blows up geometrically in just few iterations, see e.g. [7].

A black and white (B & W) (256 $\times$ 256) Picture 1(a) was chosen for its visual simplicity and for the clear dependence of its information content on the presence of singularities. (One can see the difficulties involved in writing a program to count the candies just from the image P1(b)). Picture 1(b) is the result of blurring by iterations of the diffusion equation.

Pictures 1(c), 1(d) correspond to

$$N_s = 9, 18.$$

An excellent, non-oscillatory piecewise linear reconstruction is evident.

Pictures 2(a), (b), (c) are the enhancement procedures on a (512 $\times$ 512) B & W "Tank" image: $N_d = 8, N_s = 13$.

The black and white 256 $\times$ 256 "clock" image (Picture 3(a), (b)) is chosen because it has a great deal of small details, including easily perturbed numerals on the clock's face. In this experiment the enhancement of the original image is performed, i.e. $N_d = 0$, $N_s = 5$. The procedure seems to resolve the image beyond its original fidelity, revealing for instance small details on the background photograph. The appearance of "jagged" edges simply means that edges get too compressed for the initial resolution.

The black and white (256 × 256) Picture 4(a), (b), (c) with $N_d = 0$, $N_s = 5, 11$ suggest resolution beyond the original optical limit. In particular a small "gate" appears in the white building on the background, which was not initially apparent there.

Finally Picture 5(a), (b), (c) demonstrate color enhancement on a (512 × 512) 24 B/pixel image of a lake. Here $N_d = 15$ and $N_s = 5$. Each separate color plane was shock filtered.

An interesting observation here is that Picture 5(c) appears to be an "impressionistic" version of the original. This "painting" like quality comes from the fact that the shock filter (3.7) does not restore details beyond the scales lost in the diffusion process (i.e. features whose edges are not detected by the $\tilde{F}(u)$), yet all the higher scales get perfectly enhanced. Thus the result looks like a painting – not a blur!

Appendix

In [15] a modification of Burgers' equation was used as an enhancement mechanism.

The differential equation used to enhance images was

$$u_t - f(u_x)|u_x|u = \epsilon u_{xx},\ \epsilon > 0 \tag{A1}$$

Here $f(u_x)$ was a "threshold" type of function and ϵ is quite small. If we set $\epsilon = 0$ and let $f(u_x)u$ be replaced by $-F(u_{xx})$ we arrive at (2.19).

The numerical results associated with (A1) showed some impressive denoising and deblurring. However there are two problems with this model. One is a lack of symmetry – minima and maxima are enhanced differently. The second is that, as $t \to \infty$, the evolution operator generally leads to trivial results.

As a mathematical model, it served to lead us to the present enhancement procedure. We replaced extrema oriented reconstruction by feature oriented reconstruction.

Acknowledgement: The first author would like to thank Al Barr, Jim Kajiya and Sandy Frey for providing support and a good computing environment.

Bibliography

[1] Chakravarthy, S.R. and S. Osher, *Computing with high-resolution upwind schemes for hyperbolic equations*, in Lectures in Applied Mathematics, V.22, #1, A.M.S., Providences (1985), pp. 57-86, editors: B.E. Engquist, S. Osher, and R.C.J. Somerville.

[2] Godunov, S.K., *A finite difference method for the numerical computation and discontinuous solutions of the equations of fluid dynamics*, Mat. Sb., 047, (1959) pp. 271-290.

[3] Grayson, M., *A short note on the evolution of surfaces via mean curvature*, Stanford University Math. Dept. preprint, (1987).

[4] Haralich, R., *Digital step edges from zero crossings of second directional derivatives*, IEEE Trans. on Pattern analysis and Machine Intelligence, V.1, PAMI-6, No. 1, Janury 1984, pp. 58-68.

[5] Harten, A., Engquist, B., Osher, S., and S.R. Chakravarthy, *Uniformly high order accurate essentially non-oscillatory schemes, III*, J. Comp. Physics, V.71, (1987) pp. 231-303.

[6] Harten, A., Hyman, J.M., and P.D. Lax, *On finite difference approximations and entropy conditions for shocks*, Comm. Pure. Appl. Math., V.29, (1976) pp. 297-322.

[7] Kreiss, H.-O., and J. Oliger, *Methods for the approximate solution of time dependent problems*, GARP Publication Series #10, (1973).

[8] Lax, P.D. and B. Wendroff, *Systems of conservation laws*, Comm. Pure Appl. Math., 12, (1960) pp. 217-237.

[9] Majda, A., McDonough, J., and S. Osher, *The Fourier method for nonsmooth initial data*, Math. Comp. **22** (1978) pp. 1041-1081.

[10] Marr, D. and E. Hildreth, *Theory of edge detection*, Proc. Royal Soc. London B. **207**, (1980) pp. 187-217.

[11] Osher, S., *Riemann solvers, the entropy condition and difference approximations*, SIAM J. Numer. Anal., V.27, (1984) pp. 217-235.

[12] Osher, S. and L.I. Rudin, *Feature-oriented image enhancement using shock filters*, UCLA CAM Report #89-02, (1989).

[13] Osher, S. and J.A. Sethian, *Fronts propagating with curvature dependent speed. Algorithms based on a Hamilton-Jacobi formulation*, J. Comp. Physics, V.79, (1988) pp. 12-49.

[14] Osher, S. and P.K. Sweby, *Recent developments in the numerical solution of nonlinear conservation laws*, in "The state of the art in numerical analysis", Clarendon Press, Oxford, (1987), pp. 681-701, editors: A. Iserles and M.J.D. Powell.

[15] Rudin, L., *Shock filters*, DARPA Report, Rockwell International Science Center, (1984).

[16] Rudin, L., *Images, numerical analysis of singularities, and shock filters*, Ph.D. thesis, Computer Science Dept., Caltech, Pasadena, CA, #5250:TR:87; (1987).

[17] Shu, C.W. and S. Osher, *Efficient implementation of essentially non-oscillatory shock capturing schemes*, J. Comp. Physics, V.77, (1988) pp. 439-471.

[18] Van Leer, B., *Toward the ultimate finite difference scheme, II. Monotonicity and conservation combined in a second order scheme*, J. Comp. Physics, V.14, (1974) pp. 361-370.

[19] Granlund, G.H., H. Knutsson, and R. Wilson, *Image enhancement*, in Computer Vision, North Holland, (1983) pp. 56-67.

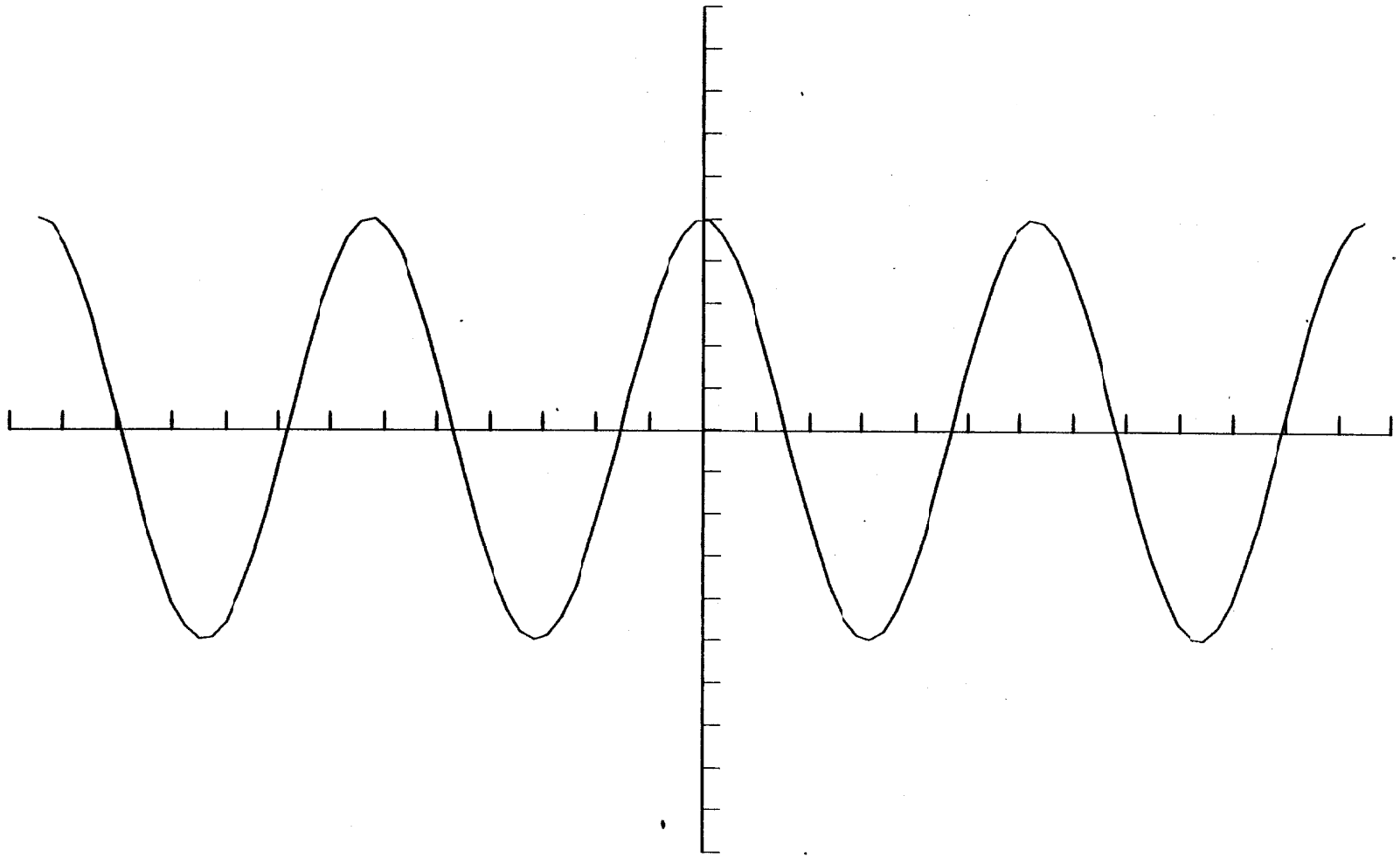

Plot 1(a)

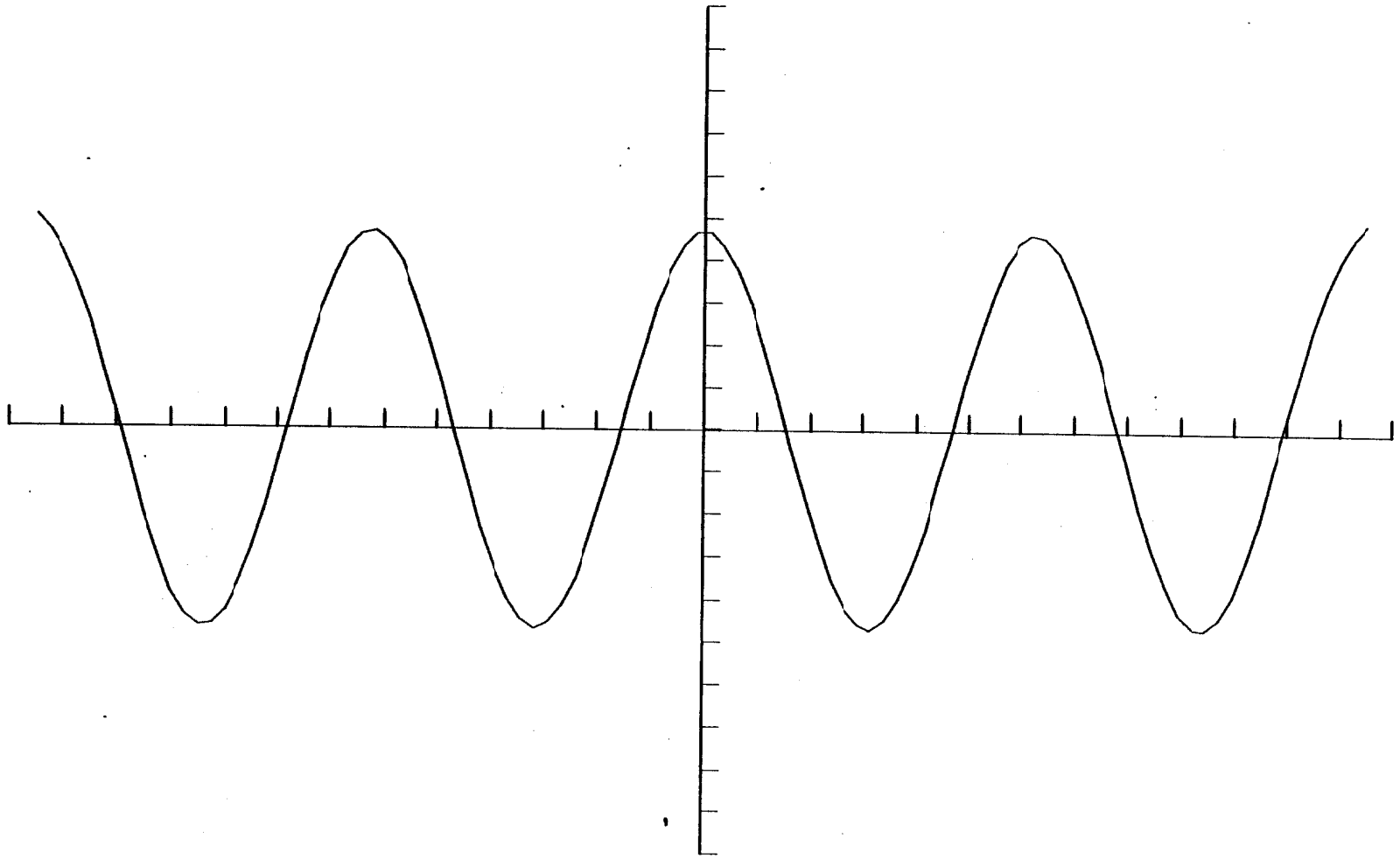

Plot 1(b)

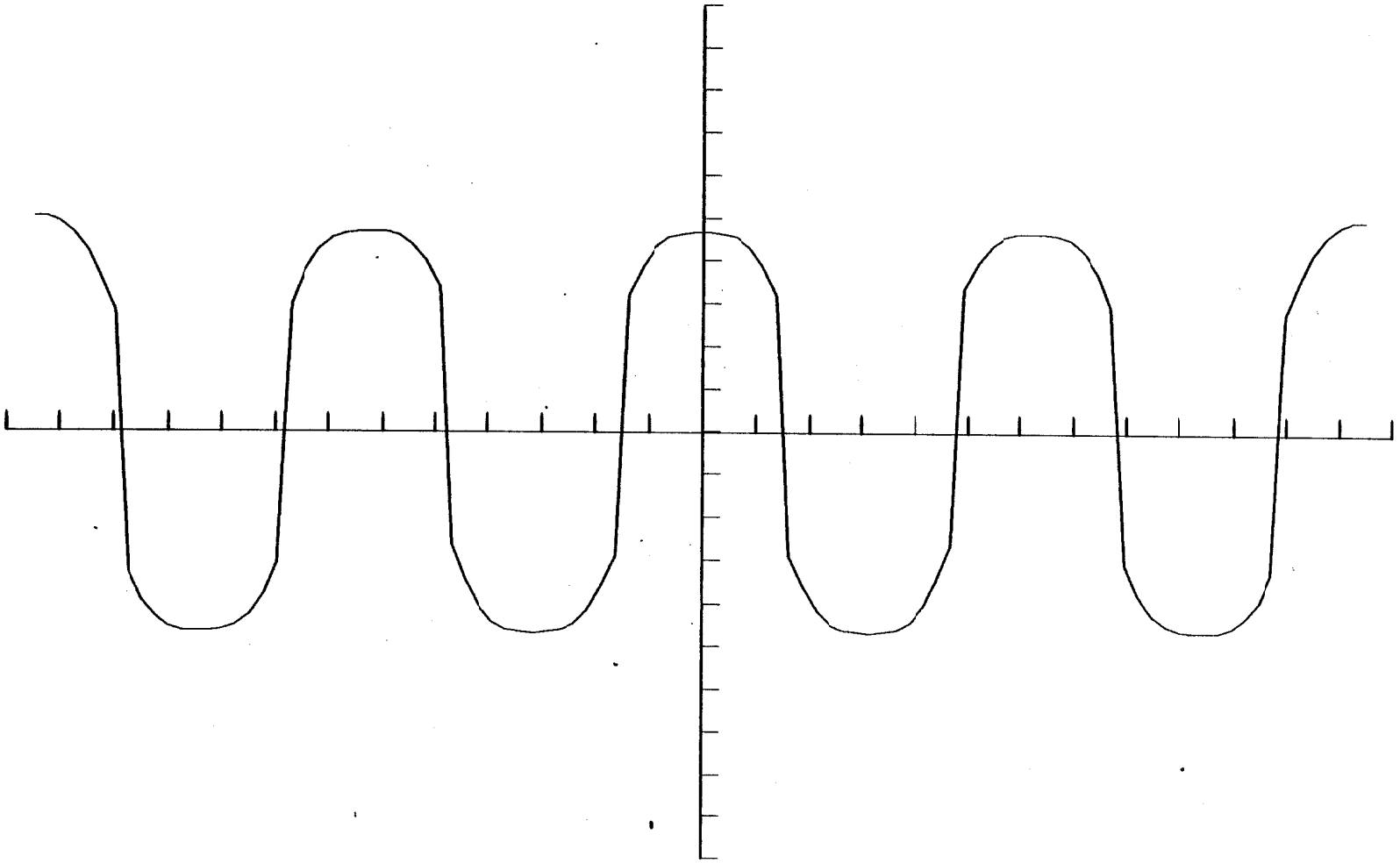

Plot 1(c)

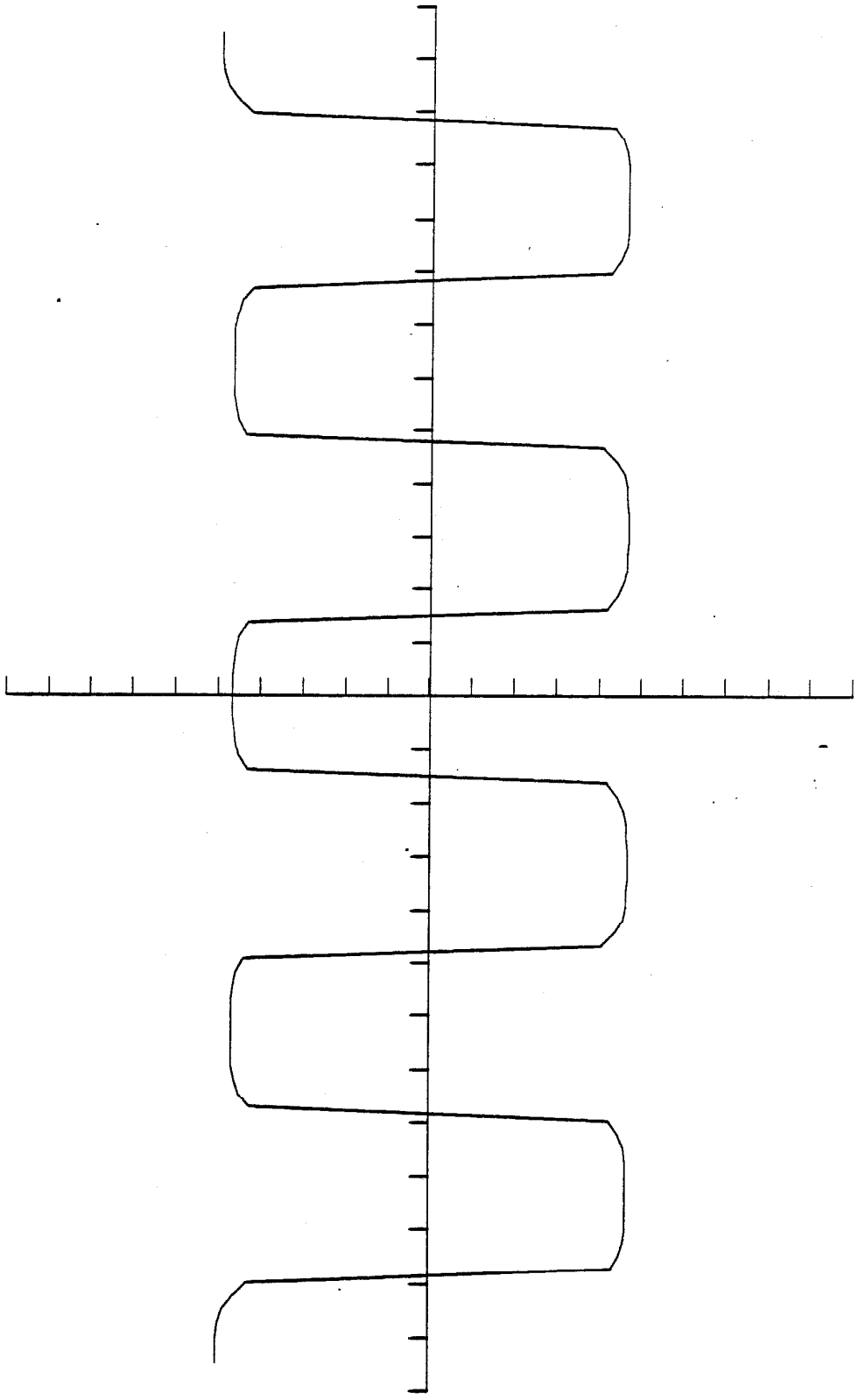

Plot 1(a)

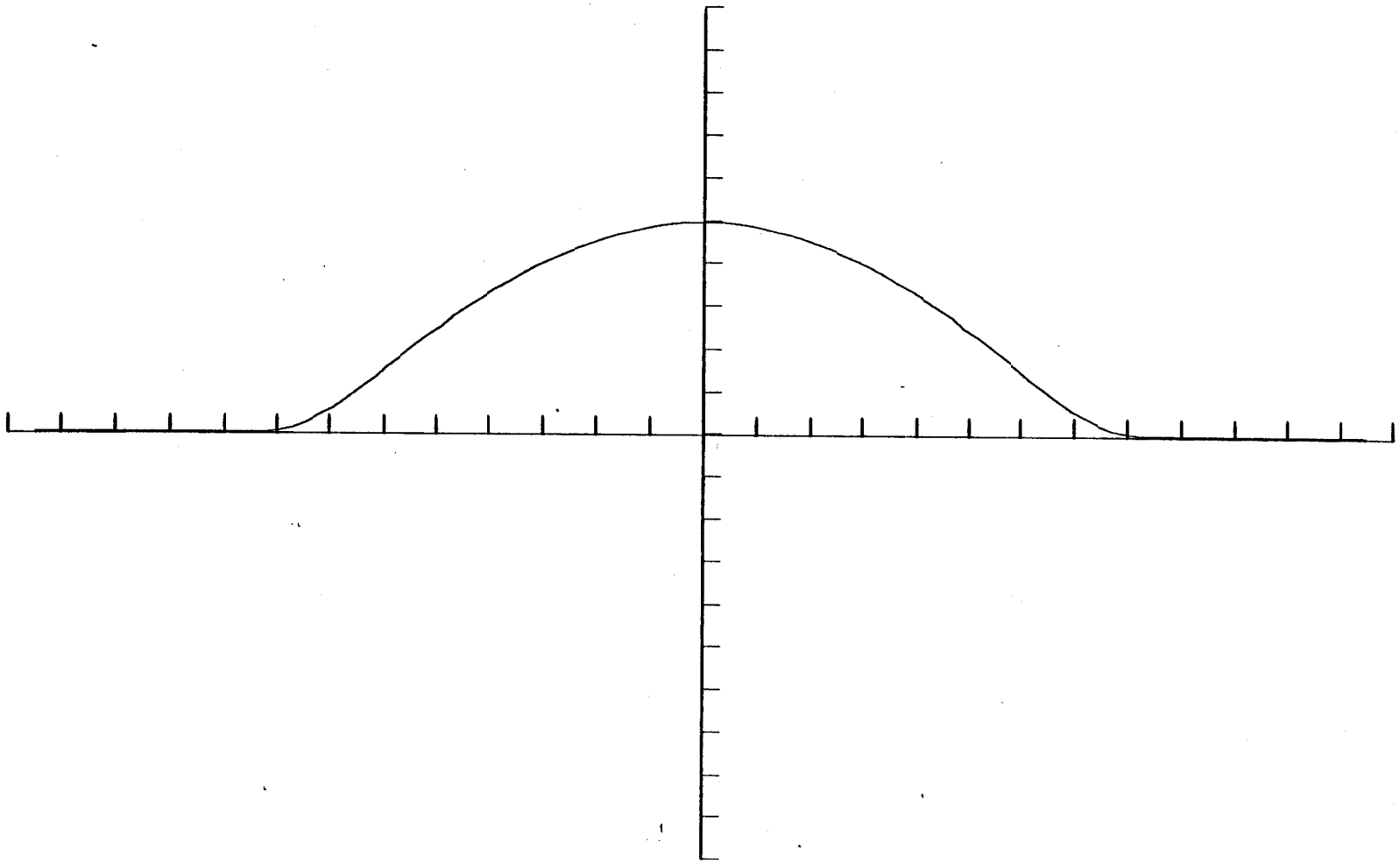

Plot 2(a)

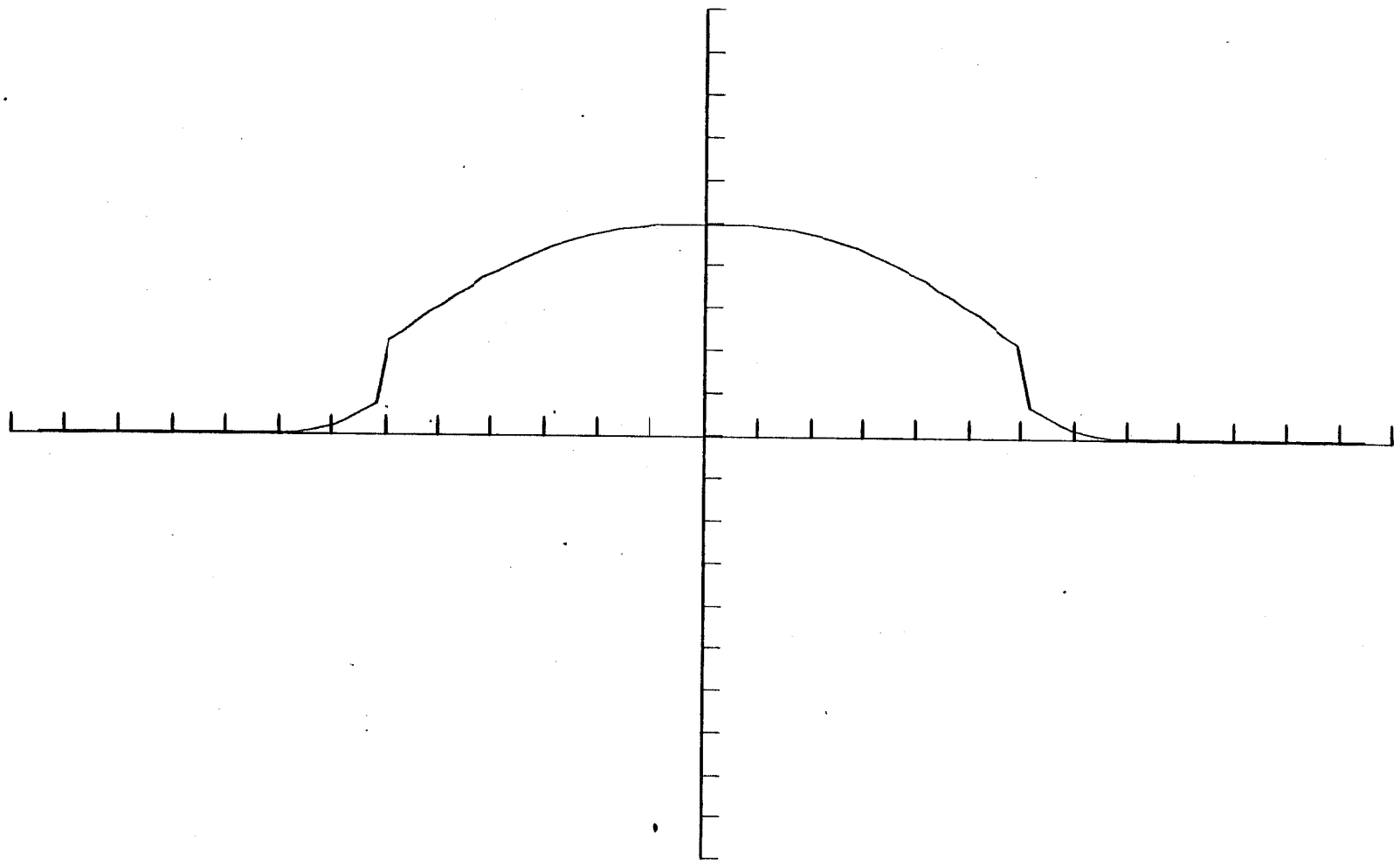

Plot 2(b)

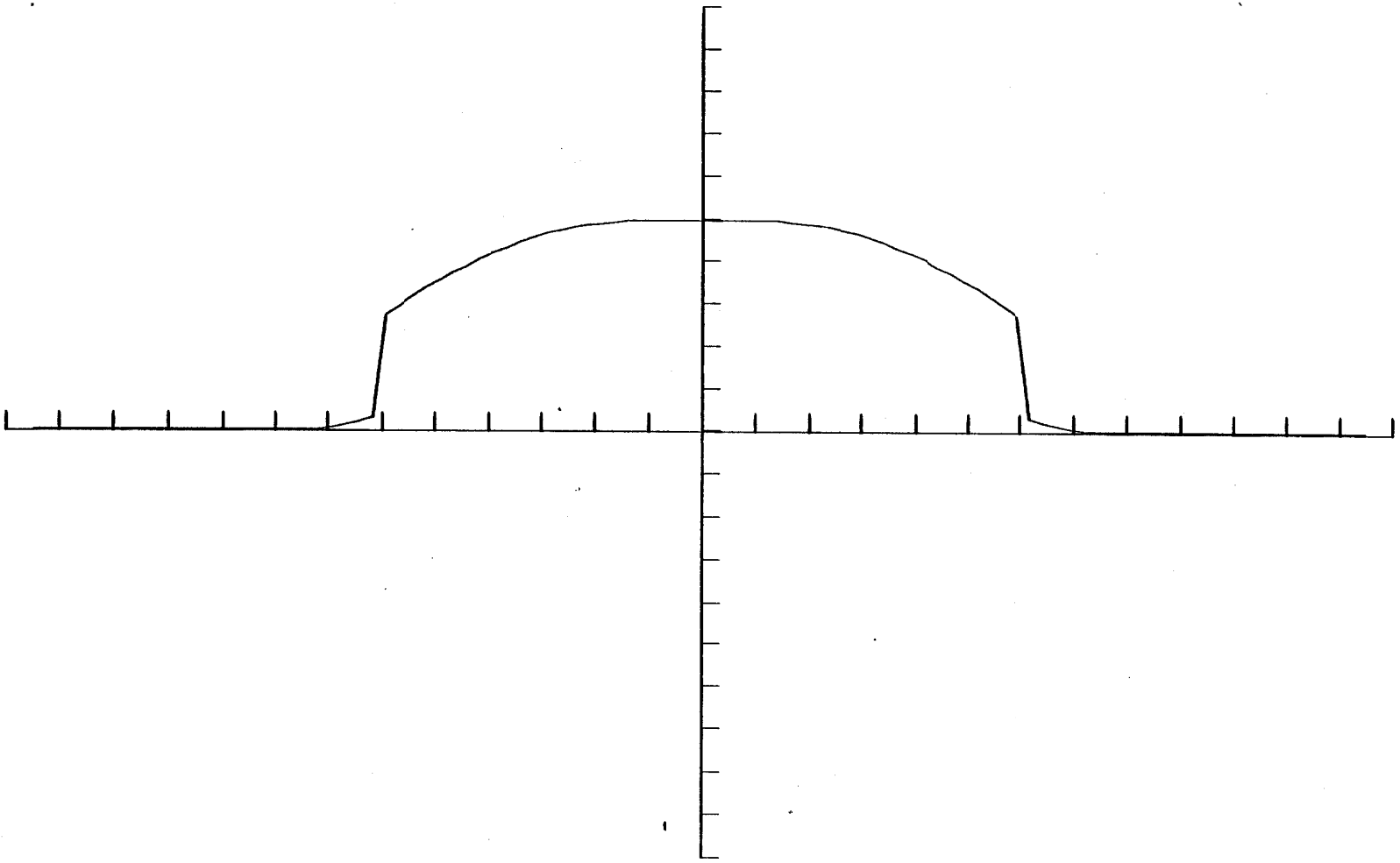

Plot 2(c)

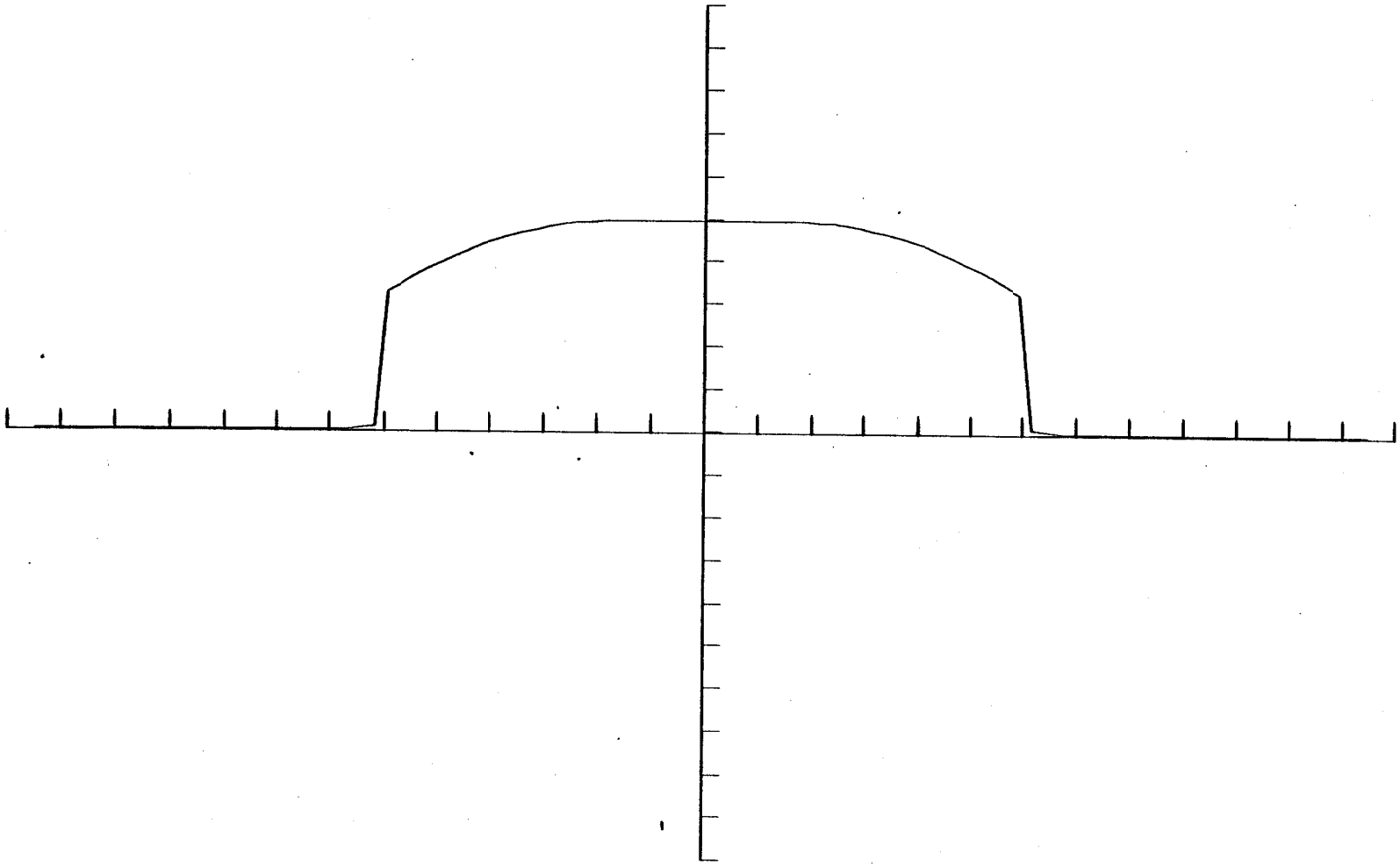

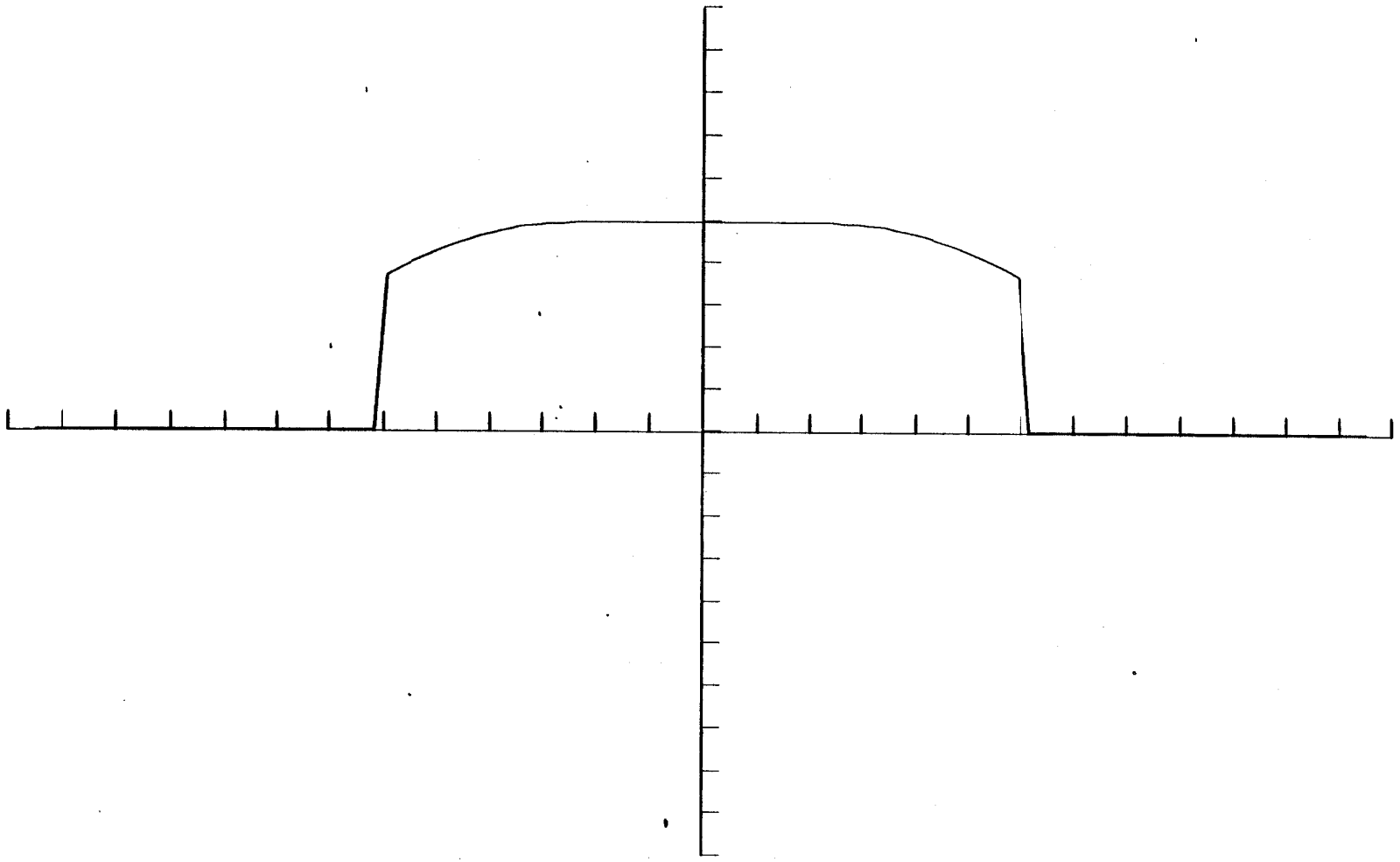

Plot 2(a)

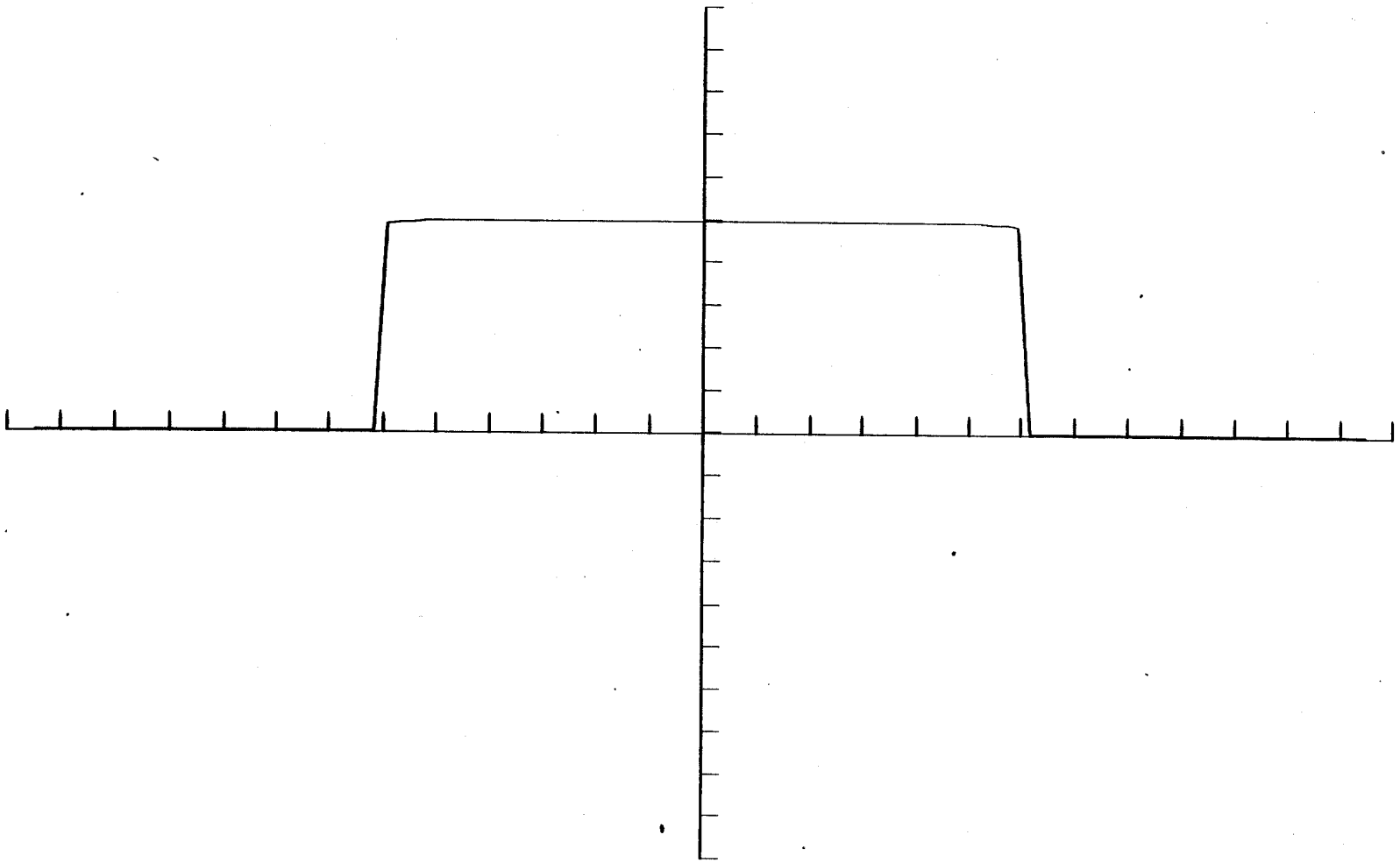

Plot 2(f)

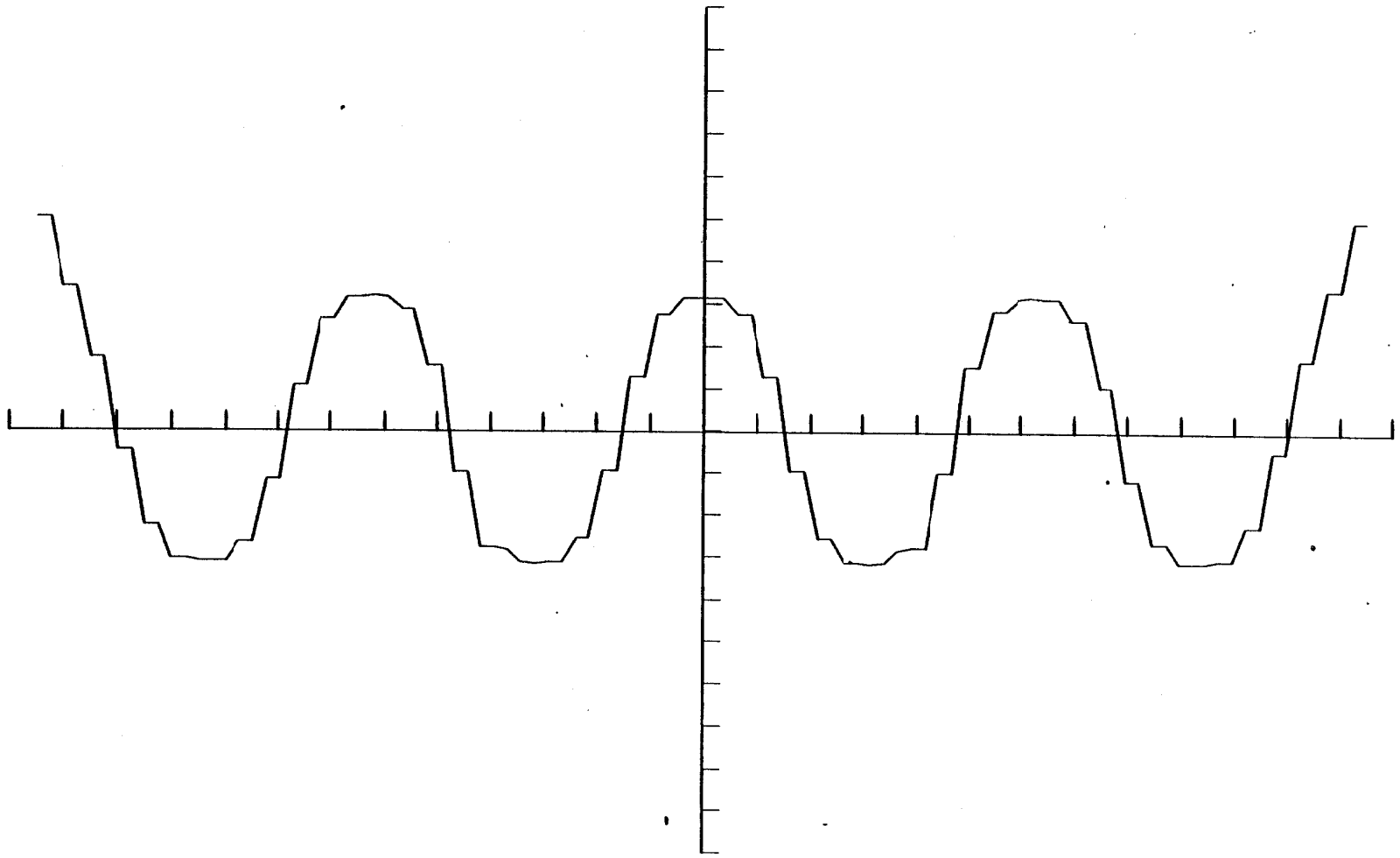

Plot 3

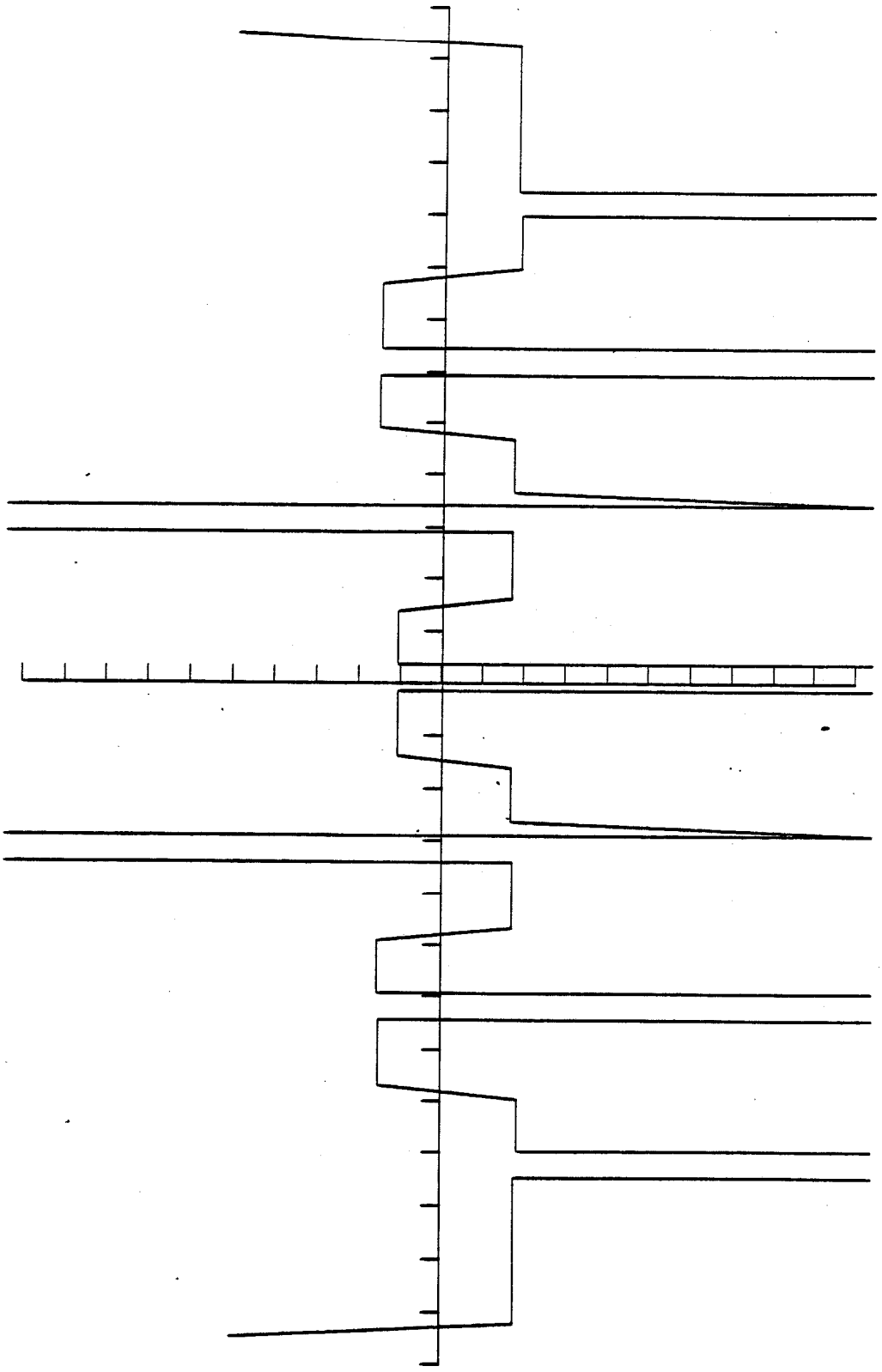

Plot 4

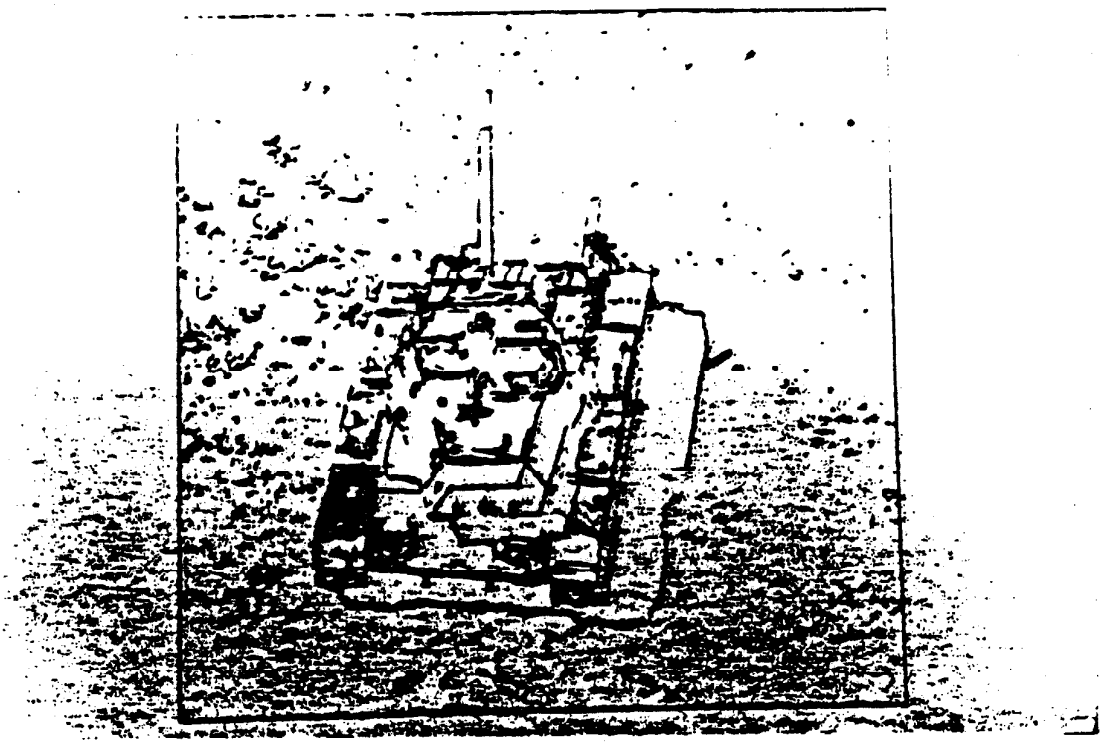

Picture 0

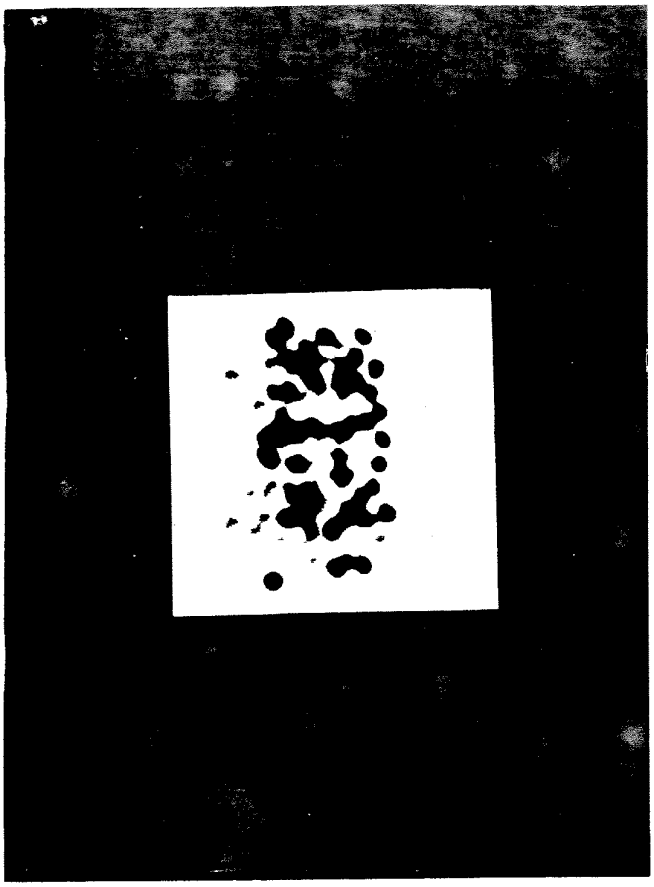

Picture 1(a)

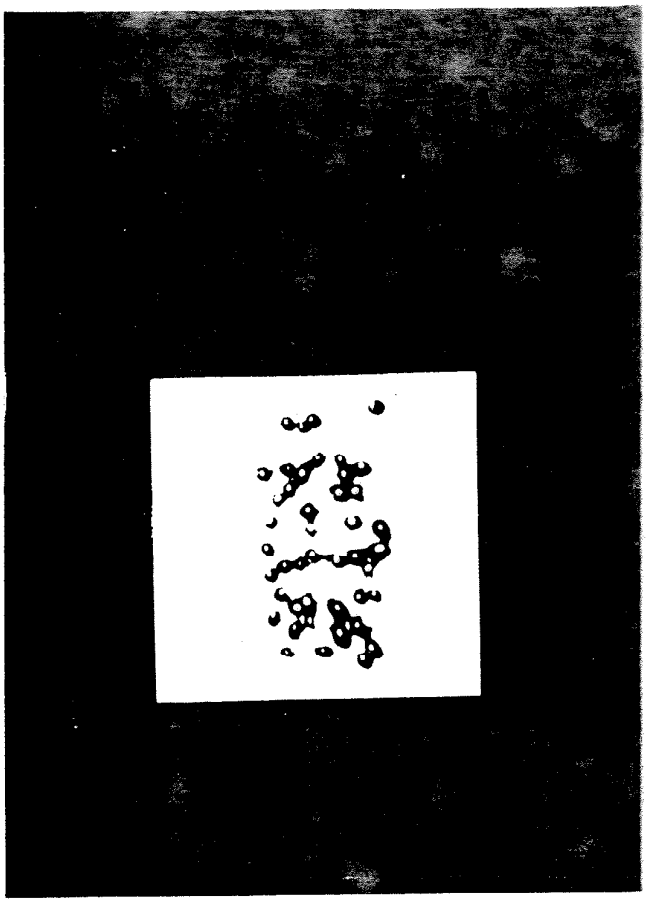

Picture 1(b)

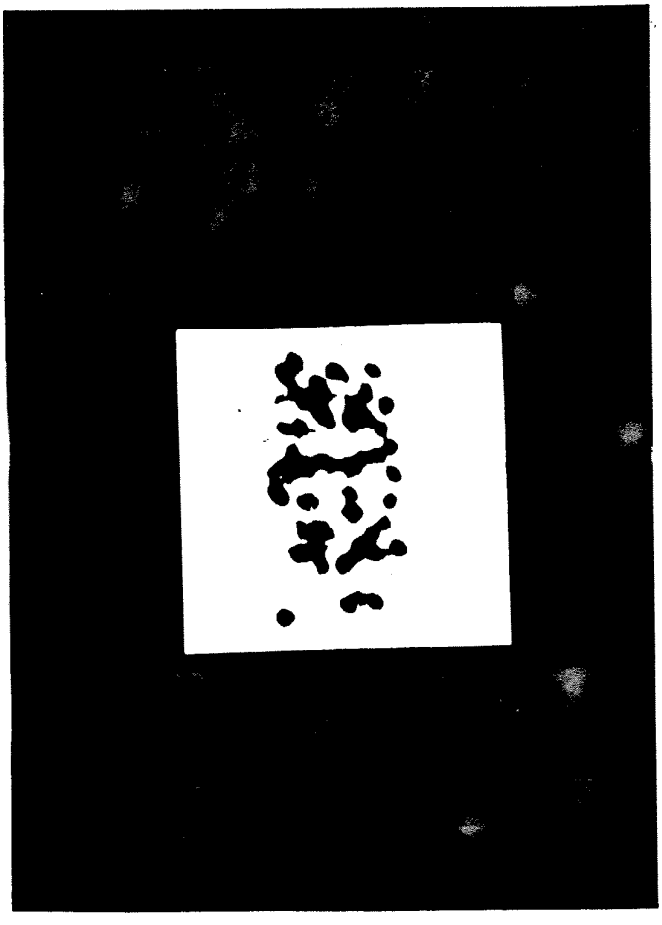

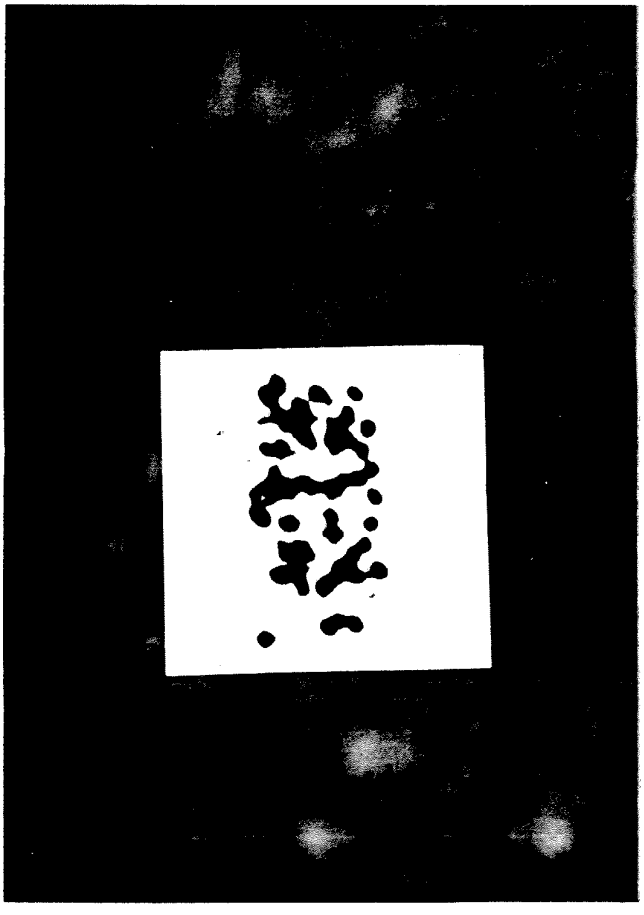

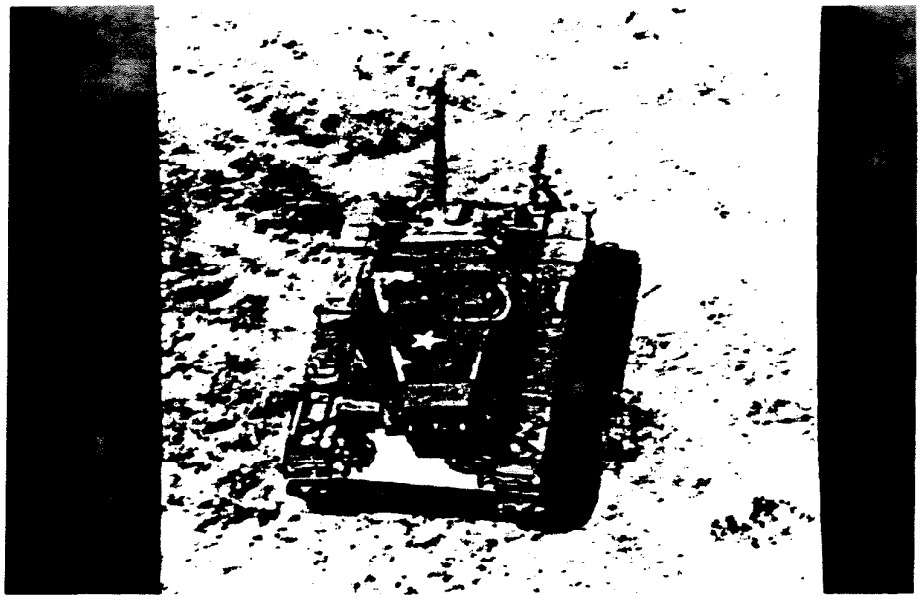

Picture 2(a)

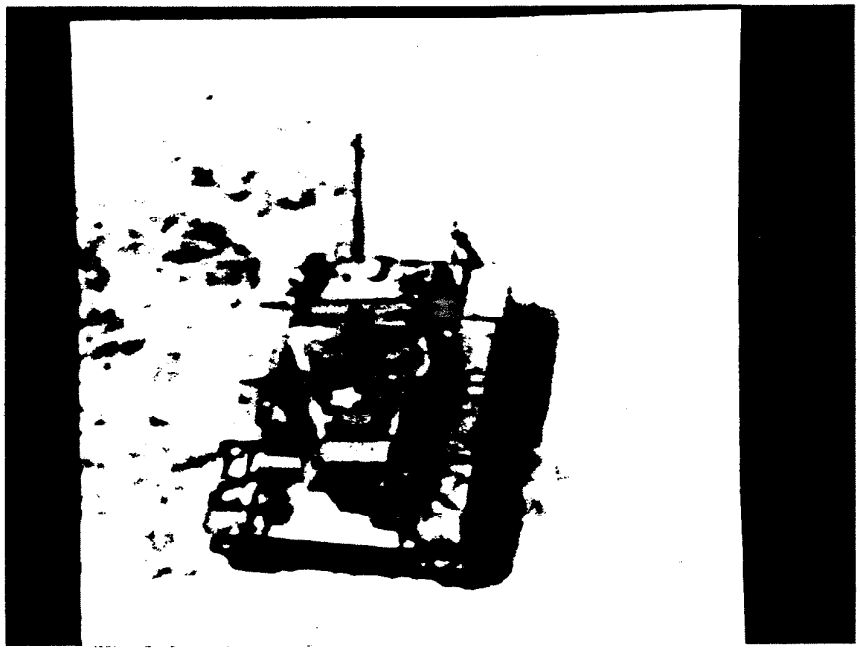

Picture 2(b)

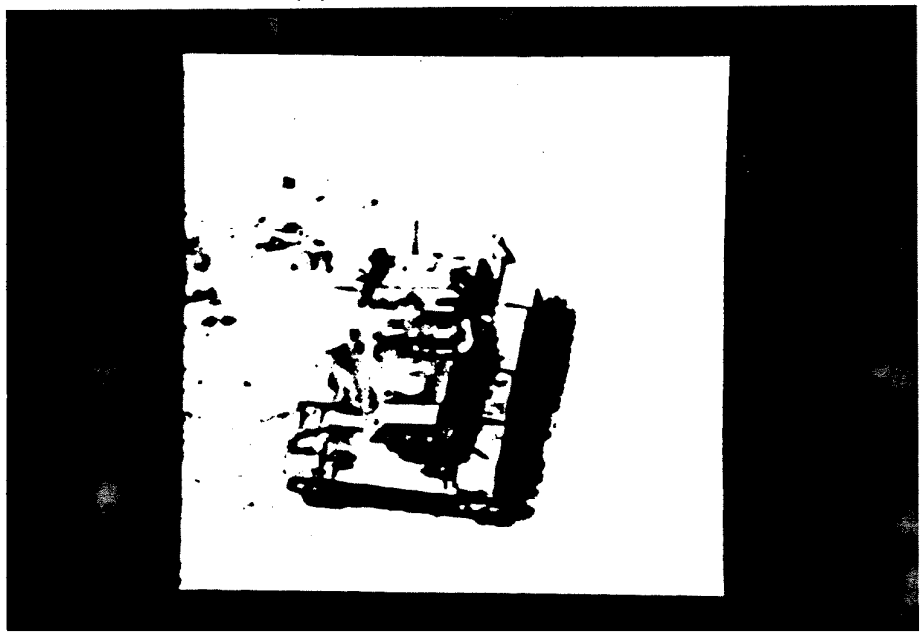

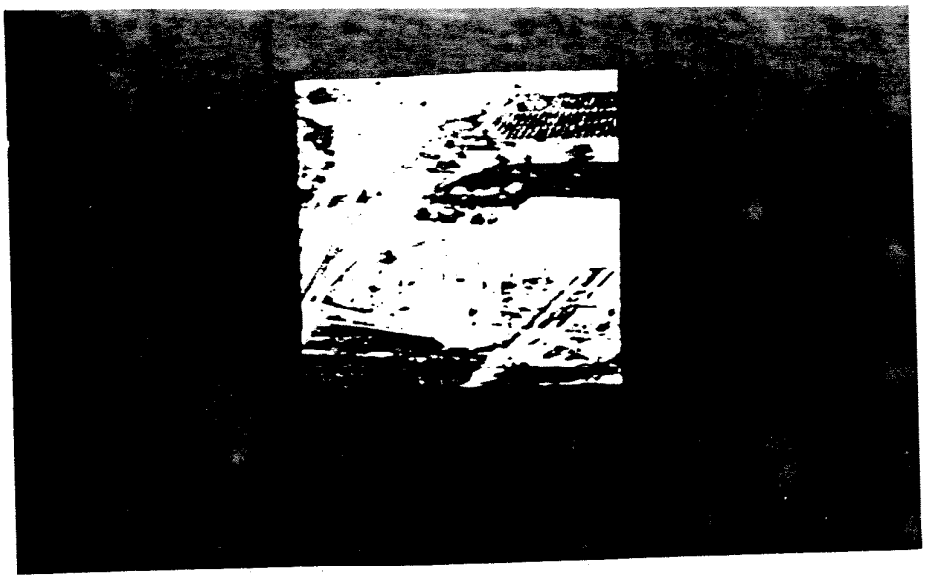

Picture 3(a)

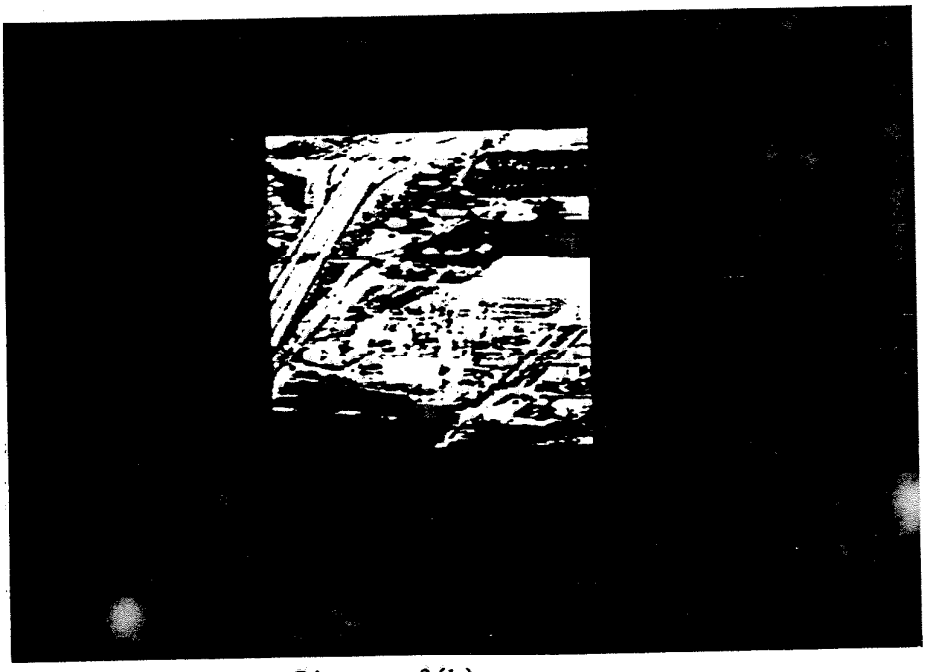

Picture 3(b)

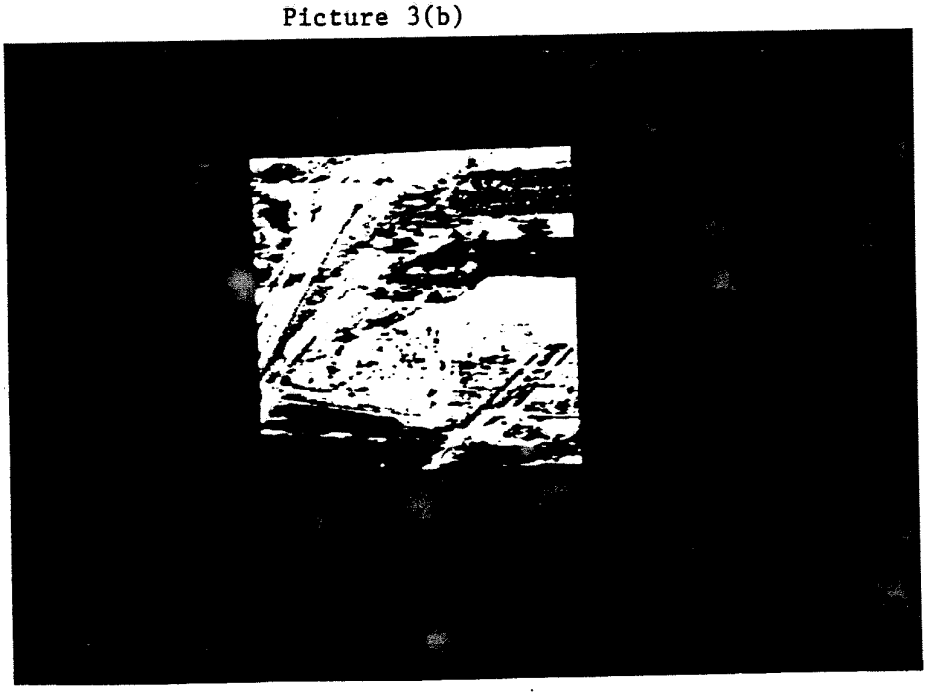

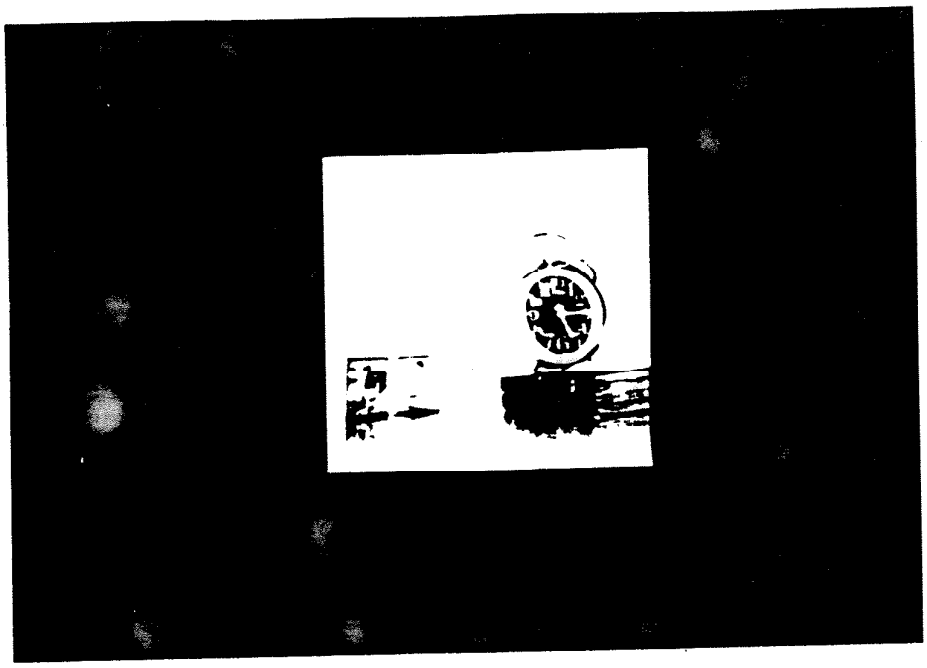

Picture 4(a)

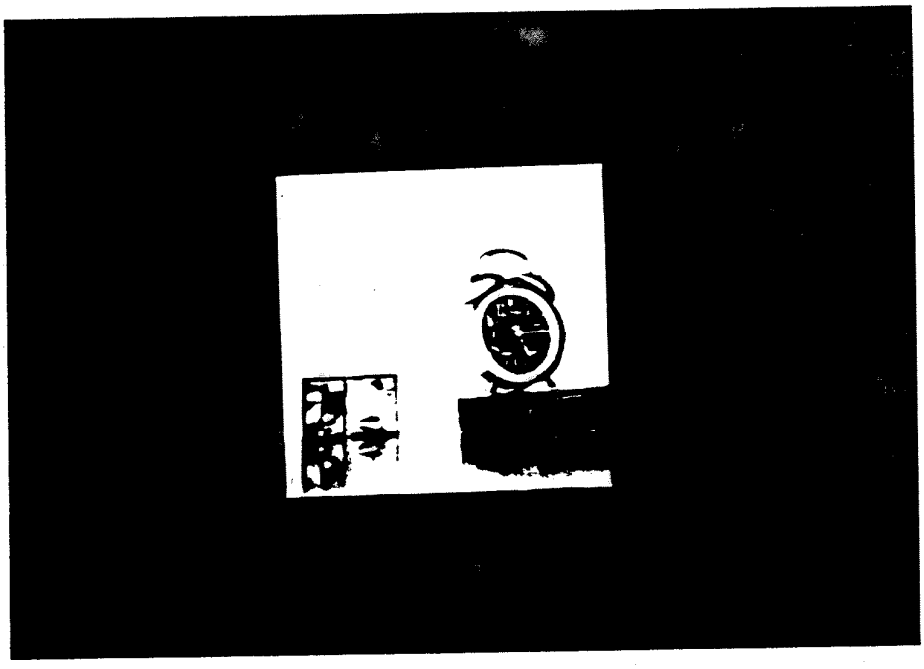

Picture 4(b)

Picture 5(a)

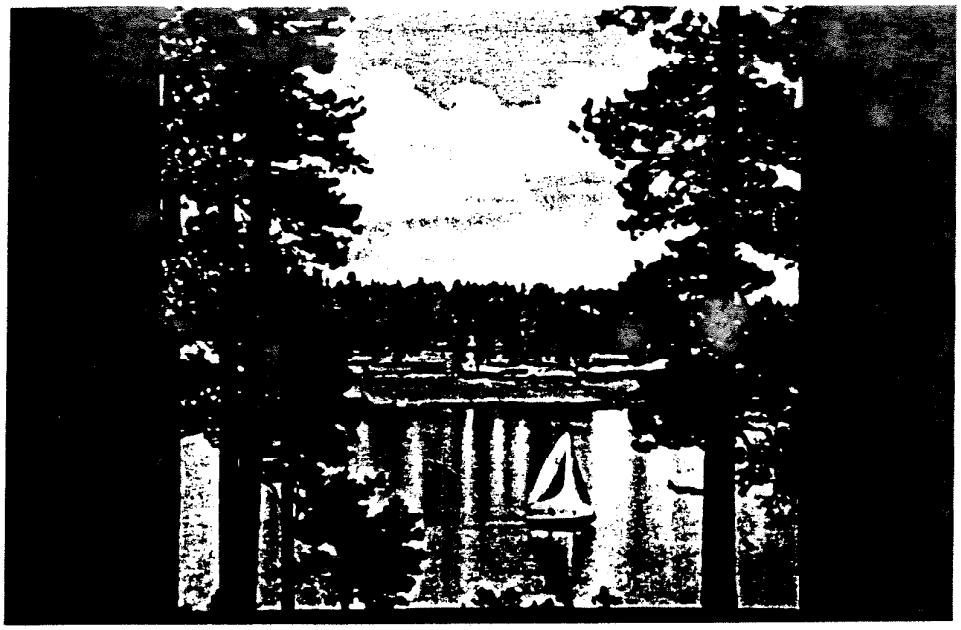

Picture 5(b)

Picture 5(c)

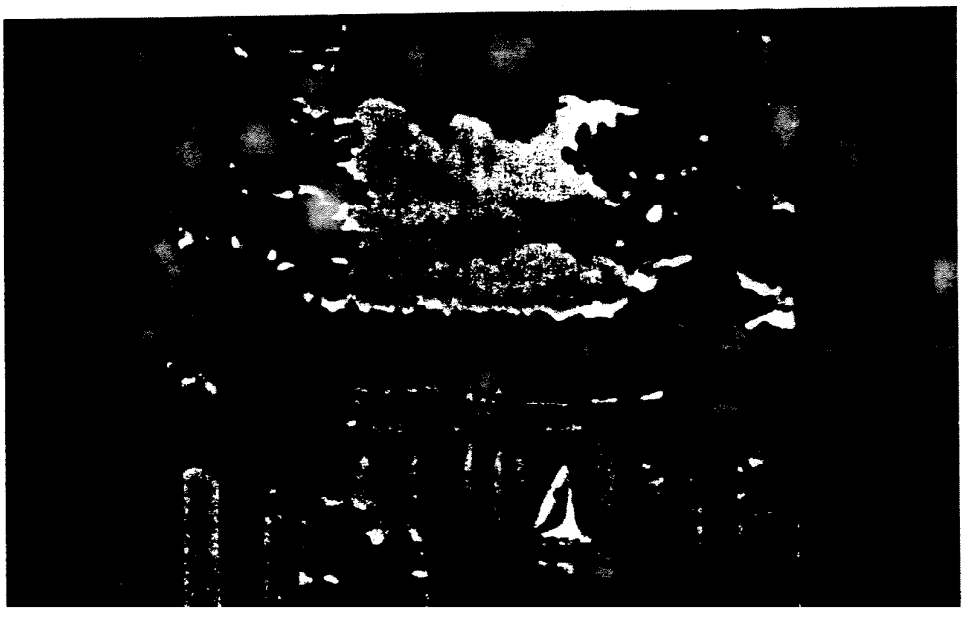

Keywords: Shock filters, total variation, image enhancement, deconvolution.

AMS MOS Classification: Primary 68U10; Secondary 65M05, 65M10